NAVAL POSTGRADUATE SCHOOL
MONTEREY, CALIFORNIA

THESIS

AIRY FUNCTIONS AND THE RECURSIVE RAY ACOUSTICS ALGORITHM

by

Robert Simpson House

December, 1994

Thesis Advisor: Lawrence J. Ziomek

Approved for public release; distribution is unlimited.

REPORT DOCUMENTATION PAGE

Form Approved OMB No. 0704-0188

1. AGENCY USE ONLY *(Leave blank)*	2. REPORT DATE December 1994	3. REPORT TYPE AND DATES COVERED Master's Thesis

4. TITLE AND SUBTITLE
AIRY FUNCTIONS AND THE RECURSIVE RAY ACOUSTICS ALGORITHM

5. FUNDING NUMBERS

6. AUTHOR(s) House, Robert, S.

7. PERFORMING ORGANIZATION NAME(S) AND ADDRESS(ES)
Naval Post Graduate School
Monterey CA 93943-5000

8. PERFORMING ORGANIZATION REPORT NUMBER

9. SPONSORING/MONITORING AGENCY NAME(S) AND ADDRESS(ES)

10. SPONSORING/MONITORING AGENCY REPORT NUMBER

11. SUPPLEMENTARY NOTES The views expressed in this thesis are those of the author and do not reflect the official policy or position of the Department of Defense or the U.S. Government.

12a. DISTRIBUTION/AVAILABILITY STATEMENT
Approved for public release; distribution unlimited

12b. DISTRIBUTION CODE

13. ABSTRACT *(maximum 200 words)*

Two main problems are analyzed and discussed in this thesis. First, a detailed derivation of the exact solution for the inhomogeneous Helmholtz equation for a free-space propagation problem when the square of the index of refraction is a linear function of depth and the input is an omnidirectional point source is performed and discussed. The exact solution is in terms of Airy and Bairy functions. Second, the accuracy of the Recursive Ray Acoustics (RRA) Algorithm was tested by generating test cases using a sound-speed profile with the square of the index of refraction a linear function of depth. The acoustic pressure (amplitude and phase) calculations obtained from the RRA Algorithm were then compared to the exact "Airy function" solution. Computer simulation results indicate that both solutions are in good agreement.

14. SUBJECT TERMS
The inhomgeneous Helmholtz equation for a free-space propagation problem, Airy and Bairy function solutions and the Recursive Ray Acoustics Algorithm

15. NUMBER OF PAGES
74

16. PRICE CODE

17. SECURITY CLASSIFICATION OF REPORT	18. SECURITY CLASSIFICATION OF THIS PAGE	19. SECURITY CLASSIFICATION OF ABSTRACT	20. LIMITATION OF ABSTRACT
Unclassified	Unclassified	Unclassified	UL

NSN 7540-01-280-5500

Standard Form 298 (Rev. 2-89)
Prescribed by ANSI Std. 239-18

Approved for public release; distribution is unlimited.

AIRY FUNCTIONS AND
THE RECURSIVE RAY ACOUSTICS
ALGORITHM

by

Robert S. House
Lieutenant , United States Navy
E.E., Auburn University, 1988

Submitted in partial fulfillment
of the requirements for the degree of

MASTER OF SCIENCE IN ELECTRICAL ENGINEERING

from the

NAVAL POSTGRADUATE SCHOOL
December 1994

Author: Robert S. House
Robert S. House

Approved by: Lawrence J. Ziomek
Lawrence J. Ziomek, Thesis Advisor

Clyde Scandrett, Second Reader

Charles W. Therrien (for)
Michael A. Morgan, Chairman,
Department of Electrical and Computer Engineering

ABSTRACT

Two main problems are analyzed and discussed in this thesis. First, a detailed derivation of the exact solution for the inhomogeneous Helmholtz equation for a free-space propagation problem when the square of the index of refraction is a linear function of depth and the input is an omnidirectional point source is performed and discussed. The exact solution is in terms of Airy and Bairy functions. Second, the accuracy of the Recursive Ray Acoustics (RRA) Algorithm was tested by generating test cases using a sound-speed profile with the square of the index of refraction a linear function of depth. The acoustic pressure (amplitude and phase) calculations obtained from the RRA Algorithm were then compared to the exact "Airy function" solution. Computer simulation results indicate that both solutions are in good agreement.

TABLE OF CONTENTS

I. INTRODUCTION

This thesis has two primary goals. The first goal is to derive and document the solution to the three-dimensional inhomogeneous Helmholtz equation for a free-space propagation problem when the square of the index of refraction is a linear function of depth. Given this type of ocean medium, the inhomogeneous Helmholtz equation has an exact solution in terms of Airy functions. This exact "Airy function" solution will be incorporated into the computer program Linear Space-Variant Ocean (LSVOCN) as an additional ocean-medium transfer function. The second goal of this thesis is to further test the Recursive Ray Acoustics (RRA) Algorithm by comparing the magnitude and phase of the acoustic pressure calculated along a ray path by the RRA Algorithm with the magnitude and phase calculated by LSVOCN.

The first step in this process requires a careful derivation of the solution to the three-dimensional inhomogeneous Helmholtz equation for a free-space propagation problem when the square of the index of refraction is a linear function of depth. This derivation will be discussed in detail in Chapter II which is divided into three main sections. Section A defines the three-dimensional inhomogeneous Helmholtz equation to be solved. (By using a zeroth-order Hankel transform, the solution process is simplified to solving a one-dimensional inhomogeneous ordinary differential equation vice a three-dimensional inhomogeneous Helmholtz equation). Section B defines the mathematical formula used to model the square of the index of refraction as a linear function of depth. Section C documents the three steps that lead to the final solution of the inhomogeneous Helmholtz equation.

First, the description of the sound-speed profile is defined. This description allows us to solve for the two constants in the equation for the square of the index of refraction as a linear function of depth. Second, the homogeneous depth equation is manipulated into the form of Airy's differential equation and then solved in terms of Airy and Bairy functions. Third, the solution of the inhomogeneous depth equation is obtained by applying the appropriate boundary conditions at the source.

The solution to the inhomogeneous Helmholtz equation is divided into two cases. In case one, the square of the index of refraction has a negative gradient. This case is further subdivided into a solution for the receiver depth equal to or above the source depth, and a solution for the receiver depth below the source depth. In case two, the square of the index of refraction has a positive gradient, and again a solution for the receiver depth equal to or above the source depth, and a solution for the receiver depth below the source depth are found.

Chapter III is divided into three sections. Section A discusses the numerical techniques used in the process of converting the Airy function solution into working FORTRAN computer code used by LSVOCN, and defines the Green's function used to test LSVOCN. Before testing of the RRA Algorithm began, a comparison was made of the output of LSVOCN, using the above derived Airy function solution, with a test case, in an effort to validate the FORTRAN computer code. The simplest test case considered compared the magnitude and phase of the time-independent free-space Green's function for an isospeed medium with the output from LSVOCN.

Section B of Chapter III discusses the three different Green's function test cases that were used to test LSVOCN. These are: (1) Green's function test case with the source sound-speed varied such that the modeled ocean medium approached an isospeed medium in order to compare the magnitude and phase of the Green's function with LSVOCN, (2) Green's function test case with the horizontal range varied while maintaining the receiver at the source depth, thus simulating an isospeed ocean medium for comparison of the Green's function magnitude and phase with LSVOCN, and (3) Green's function test case with the receiver depth varied above and below the source depth by one-half meter allowing for an approximate comparison of the Green's function magnitude and phase with LSVOCN. In each test case, the change in sound speed between the source and receiver was small enough to approximate an isospeed ocean medium.

Section C of Chapter III focuses on the validation of the predicted values for the magnitude and phase of the acoustic pressure along a ray path given by the RRA

Algorithm. This is done by propagating sound rays at various launch angles using negative and positive gradients for the index of refraction profile. The horizontal range and depth coordinates of selected points along these ray paths have been recorded and will become the receiver horizontal range and depth coordinates used later as inputs to LSVOCN. The magnitude and phase values calculated by LSVOCN are then compared to the corresponding magnitude and phase values obtained from the RRA Algorithm for validation purposes.

Chapter IV summarizes the numerical problems encountered during the validation process, states conclusions as well as recommendations for future research.

II. AIRY FUNCTION SOLUTION OF THE INHOMOGENEOUS HELMHOLTZ EQUATION

A. THE INHOMOGENEOUS HELMHOLTZ WAVE EQUATION

In this chapter we shall derive a solution for the following inhomogeneous Helmholtz equation in cylindrical coordinates (r, ϕ ,y), shown in Fig. 1:

$$\frac{\partial^2}{\partial r^2}\varphi_f(r,y)+\frac{1}{r}\frac{\partial}{\partial r}\varphi_f(r,y)+\frac{\partial^2}{\partial y^2}\varphi_f(r,y)+k^2(y)\varphi_f(r,y)=\frac{\delta(r)}{2\pi r}\delta(y-y_0) \qquad (2.1)$$

where the velocity potential $\varphi_f(r,y)$ is axisymmetric (i.e., independent of the azimuthal angle ϕ),

$$k(y)=\frac{2\pi f}{c(y)} \qquad (2.2)$$

is the depth-dependent wave number, $c(y)$ is the depth-dependent speed of sound, and the impulse functions on the right-hand side of Eq.(2.1) represent a unit amplitude, omnidirectional point source at $r=0$ and $y=y_0$.

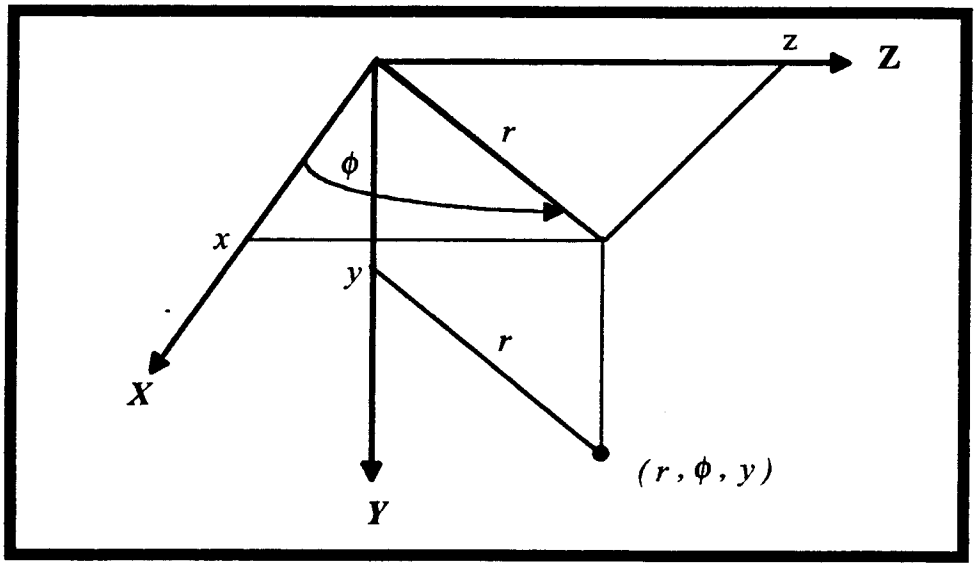

Figure 1. Illustration of problem geometry.

The solution $\varphi_f(r,y)$ of Eq.(2.1) can be expressed as an inverse zeroth-order Hankel transform as follows, see [Ref. 2, Appendix 3C]:

$$\varphi_f(r,y) = H_0^{-1}\{\Phi_f(k_r,y)\} = \int_0^\infty \Phi_f(k_r,y) J_0(k_r r) k_r dk_r \tag{2.3}$$

where

$$\Phi_f(k_r,y) = H_0\{\varphi_f(r,y)\} = \int_0^\infty \varphi_f(r,y) J_0(k_r r) r dr \tag{2.4}$$

is the forward zeroth-order Hankel transform (also known as the Fourier-Bessel transform) of $\varphi_f(r,y)$. Therefore, if we can find $\Phi_f(k_r,y)$, then substituting $\Phi_f(k_r,y)$ into Eq.(2.3) will yield a solution of Eq.(2.1).

Since

$$H_0\left(\frac{\partial^2}{\partial r^2}\varphi_f(r,y) + \frac{1}{r}\frac{\partial}{\partial r}\varphi_f(r,y)\right) = -k_r^2 \Phi_f(k_r,y) \tag{2.5}$$

and

$$H_0\left(\frac{\delta(r)}{r}\right) = 1, \tag{2.6}$$

taking the zeroth-order Hankel transform of Eq.(2.1) yields

$$\frac{d^2}{dy^2}\Phi_f(k_r,y) + k_y^2(y)\Phi_f(k_r,y) = \frac{\delta(y-y_0)}{2\pi} \tag{2.7}$$

where

$$k_y^2(y) = k^2(y) - k_r^2. \tag{2.8}$$

In Eq.(2.8), $k_y(y)$ is the depth-dependent propagation-vector component in the Y direction and k_r is the constant propagation-vector component in the horizontal range r direction (see Fig. 2). Therefore, now we only have to solve the ordinary differential equation given by Eq.(2.7) instead of the partial differential equation given by Eq.(2.1). Substituting the solution $\Phi_f(k_r,y)$ into Eq.(2.3) yields the solution $\varphi_f(r,y)$ to Eq.(2.1).

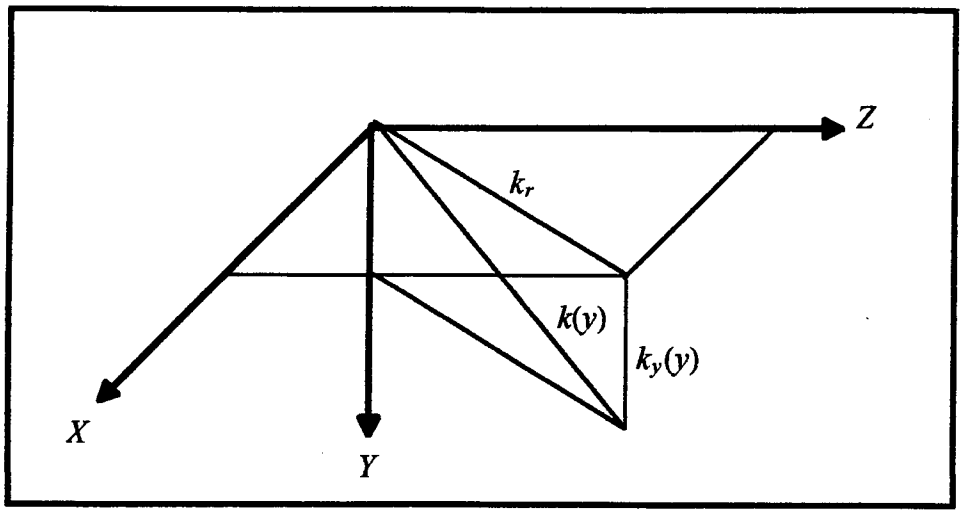

Figure 2. Illustration of the propagation-vector components k_r and $k_y(y)$ and their relationship to the wave number $k(y)$.

B. PROBLEM CONSTRAINTS

The solution of Eq.(2.1) that shall be derived is only applicable to free-space propagation when the square of the index of refraction is a linear function of depth y. The index of refraction is defined as follows:

$$n(y) = \frac{c_0}{c(y)} \tag{2.9}$$

where $c_0 = c(y_0)$ is the speed of sound (m/s) at the source depth y_0 and $c(y)$ is the speed of sound (m/s) at depth y. If we let $k_0 = k(y_0)$, then evaluating Eq.(2.2) at $y = y_0$ yields

$$k_0 = \frac{2\pi f}{c_0}. \tag{2.10}$$

Therefore, we can write that

$$k(y) = k_0 n(y) = \frac{2\pi f}{c(y)}. \tag{2.11}$$

As a result, Eq.(2.8) can be rewritten as

$$k_y^2(y) = k_0^2 n^2(y) - k_r^2. \tag{2.12}$$

To ensure that the square of the index of refraction is a linear function of depth, we define the following equation:

$$n^2(y) = a_1 y + a_0. \tag{2.13}$$

C. PROBLEM SOLUTION

Using the results from the last two sections, specifically Eq. (2.7) and (2.12), we are now ready to solve the inhomogeneous Helmholtz equation. The solution can be broken into two parts. First, determine the solution of Eq.(2.7) at $y = y_0$, i.e., solve the homogeneous equation. Solving the homogeneous equation will result in four unknowns. In order to determine these four unknowns, which is the second part of the problem, we apply the boundary conditions above and below the source and the boundary conditions at the source, i.e., at $y = y_0$. As shown in [Ref. 2, Appendix 3C], the two boundary conditions that must be satisfied at the source are continuity of acoustic pressure and discontinuity in the y component of the acoustic fluid velocity vector. With this brief introduction in mind, let us now proceed with the solution of the inhomogeneous Helmholtz equation.

1. Description of the Sound-Speed Profile

Consider a sound-speed profile where the square of the index of refraction is a linear function of depth, [see Eq.(2.13)]:

$$n^2(y) = a_1 y + a_0. \tag{2.14}$$

With the above equation in mind, we must now solve for the two unknown constants, a_0 and a_1, in order to solve Eq(2.7). Substituting Eq.(2.9) into Eq.(2.14) yields

$$\frac{c_0^2}{c^2(y)} = a_1 y + a_0. \tag{2.15}$$

Rewriting Eq.(2.15) yields

$$\frac{1}{c^2(y)} = \frac{a_1}{c_0^2} y + \frac{a_0}{c_0^2}, \tag{2.16}$$

and if we let

$$a_1' = \frac{a_1}{c_0^2} \tag{2.17}$$

and

$$a_0' = \frac{a_o}{c_0^2}, \tag{2.18}$$

then

$$\frac{1}{c^2(y)} = a_1' y + a_0'. \tag{2.19}$$

Solving for the speed of sound yields

$$c(y) = \frac{1}{\sqrt{a_1' y + a_0'}} = \frac{c_0}{\sqrt{a_1 y + a_0}}. \tag{2.20}$$

Equation (2.20) will allow the sound-speed profile to be calculated, once the unknown constants have been determined.

Evaluating Eq.(2.19) at $y = 0$ and at $y = y_0$, i.e., the source depth, yields

$$a_0' = \frac{1}{c^2(0)} \tag{2.21}$$

and

$$\frac{1}{c^2(y_0)} = a_1' y_0 + a_0', \tag{2.22}$$

respectively. Substituting Eq.(2.21) into Eq.(2.22) and solving for a_1' yields

$$a_1' = \frac{1}{y_0}\left[\frac{1}{c_0^2} - \frac{1}{c^2(0)}\right]. \tag{2.23}$$

Thus, using Eqs.(2.21), (2.23), (2.17), and (2.18), a_0 and a_l can be determined.

For our problem, we will use a source depth of y_0 = 150 meters. In order to define a sound-speed profile, we specify the sound speed (m/s) at y = 0 to be $c(0)$ = 1500 m/s. For a positive sound-speed gradient we specify the sound speed at the source depth to be c_0 = 1515 m/s. Similarly, for a negative sound-speed gradient, we specify the sound speed at the source depth to be c_0 = 1485 m/s. These sound-speed profiles, along with the corresponding index of refraction plots, are shown in Fig. 3 and Fig. 4, respectively.

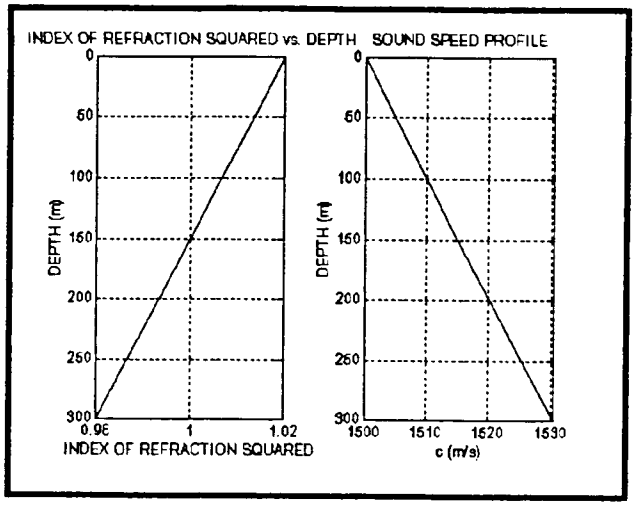

Fig. 3 Positive sound-speed gradient.

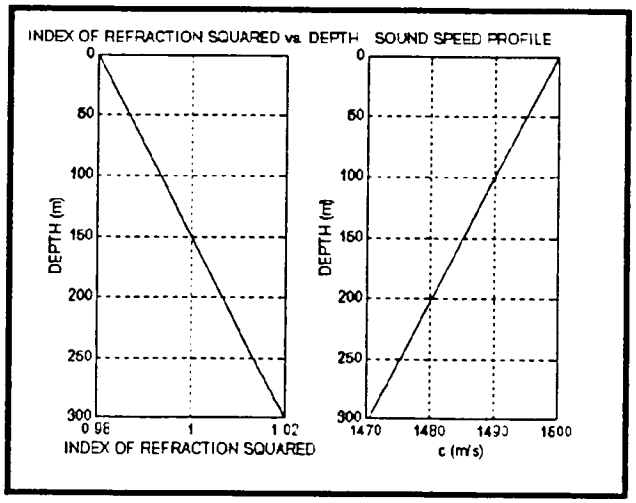

Fig. 4 Negative sound-speed gradient.

2. Solution to the Homogeneous Depth Equation

Having carefully defined the sound-speed profile, we are now ready to solve the inhomogeneous depth dependent Helmholtz equation as given by Eq. (2.7). As stated previously, the first part of the solution process is to solve the homogeneous equation where the square of the index of refraction is a linear function of depth. The homogeneous equation is

$$\frac{d^2}{dy^2}\Phi_f(k_r,y) + k_y^2(y)\Phi_f(k_r,y) = 0. \tag{2.24}$$

Substituting Eq. (2.13) into Eq. (2.12) yields

$$k_y^2(y) = k_0^2(a_1 y + a_0) - k_r^2, \tag{2.25}$$

or

$$k_y^2(y) = k_0^2 a_1 y + k_0^2 a_0 - k_r^2. \tag{2.26}$$

Substituting Eq. (2.26) into Eq. (2.24) and simplifying

$$\frac{d^2}{dy^2}\Phi_f(k_r,y) + (a_1 k_0^2 y + a_0 k_0^2 - k_r^2)\Phi_f(k_r,y) = 0. \tag{2.27}$$

If we let α_0 and α_1 be defined as

$$\alpha_0 = a_0 k_0^2 - k_r^2 \tag{2.28}$$

and

$$\alpha_1 = a_1 k_0^2, \tag{2.29}$$

then

$$\frac{d^2}{dy^2}\Phi_f(k_r,y) + (\alpha_1 y + \alpha_0)\Phi_f(k_r,y) = 0. \tag{2.30}$$

Next, we must manipulate Eq. (2.30) into the form of Airy's differential equation.

The first step in this process is to define the new term

$$\zeta(y) = \pm(\alpha_1)^{-\frac{2}{3}}(\alpha_1 y + \alpha_0). \tag{2.31}$$

Applying the chain rule yields

$$\frac{d}{dy}\Phi_f(k_r,y) = \frac{d}{d\zeta(y)}\Phi_f(k_r,y)\frac{d\zeta(y)}{dy}, \tag{2.32}$$

and since

$$\frac{d\zeta(y)}{dy} = \pm(\alpha_1)^{\frac{1}{3}}, \tag{2.33}$$

upon substituting Eq.(2.33) into Eq. (2.32), we obtain

$$\frac{d}{dy}\Phi_f(k_r,y) = \pm(\alpha_1)^{\frac{1}{3}}\frac{d}{d\zeta(y)}\Phi_f(k_r,y). \tag{2.34}$$

Applying the chain rule again yields

$$\frac{d^2}{dy^2}\Phi_f(k_r,y) = \frac{d}{dy}\frac{d}{dy}\Phi_f(k_r,y) = \frac{d}{dy}\left[\pm(\alpha_1)^{\frac{1}{3}}\frac{d}{d\zeta(y)}\Phi_f(k_r,y)\right] \tag{2.35}$$

$$= \pm(\alpha_1)^{\frac{1}{3}}\frac{d}{d\zeta(y)}\frac{d}{dy}\Phi_f(k_r,y), \tag{2.36}$$

and upon substituting Eq. (2.34) into Eq. (2.36), we obtain

$$\frac{d^2}{dy^2}\Phi_f(k_r,y) = +(\alpha_1)^{\frac{2}{3}}\frac{d^2}{d\zeta^2(y)}\Phi_f(k_r,y). \tag{2.37}$$

Combing Eqs. (2.30), (2.31), and (2.37) yields

$$+(\alpha_1)^{\frac{2}{3}}\frac{d^2}{d\zeta^2(y)}\Phi_f(k_r,y) + (\pm)(\alpha_1)^{\frac{2}{3}}\zeta(y)\Phi_f(k_r,y) = 0, \tag{2.38}$$

or

$$\frac{d^2}{d^2\zeta(y)}\Phi_f(k_r,y) \pm \zeta(y)\Phi_f(k_r,y) = 0. \tag{2.39}$$

Upon choosing the minus sign, we have Airy's differential equation:

$$\frac{d^2}{d\zeta^2(y)}\Phi_f(k_r,y) - \zeta(y)\Phi_f(k_r,y) = 0. \tag{2.40}$$

The general solution of Airy's differential equation is given by

$$\Phi_f(k_r,y) = AAi[\zeta(y)] + BBi[\zeta(y)] \text{ , for } y \le y_0 \tag{2.41}$$

$$\Phi_f(k_r,y) = CAi[\zeta(y)] + DBi[\zeta(y)] \text{ , for } y \ge y_0 \tag{2.42}$$

where Ai and Bi are the Airy and Bairy functions, and A, B, C, and D are unknown constants. Equation (2.41) and Eq.(2.42) form the solution to the depth dependent homogeneous Helmholtz equation. We have an equation with four unknown constants as a result of solving a second-order differential equation. To find these four unknown constants, we must apply the boundary conditions above and below the source and the boundary conditions at the source, as will be done in the next section.

3. Solution to the Inhomogeneous Depth Equation

In this section we will determine the general solution to the inhomogeneous depth dependent Helmholtz equation. As stated previously, in order to solve for the four unknown constants in Eq.(2.41) and Eq.(2.42), we must satisfy the boundary conditions above and below the source and the boundary conditions at the source. However, before we proceed with this solution, let us examine in detail the behavior of the functions $Ai[\zeta(y)]$ and $Bi[\zeta(y)]$ to gain insight into the solution of the problem.

By choosing the minus sign in Eq.(2.31), we can write that

$$\zeta(y) = -(\alpha_1)^{\frac{2}{3}}(\alpha_1 y + \alpha_0) \tag{2.43}$$

Because

$$k_y^2(y) = \alpha_1 y + \alpha_0, \tag{2.44}$$

Eq.(2.43) can be rewritten as

$$\zeta(y) = -(\alpha_1)^{-\frac{2}{3}} k_y^2(y). \tag{2.45}$$

Furthermore, by referring to Eq.(2.12), we can write that

$$k_y^2(y) = k_o[n^2(y) - \sin^2(\beta_o)] \tag{2.46}$$

since $k_r = k_o sin(\beta_o)$, where β_o is the launch angle, measured with respect to the positive Y axis. Values of β_o range from 0 to 180 degrees, [Ref. 2, Chapter 5]. Tables 18 through 23, located in the Appendix, contain values for $n^2(y)$, $k_y^2(y)$, and $\zeta(y)$ as a function of frequency, β_o, and depth y, for the analysis of the functions $Ai[\zeta(y)]$ and $Bi[\zeta(y)]$. The data in these tables is further displayed in graphical form in Figures 12 through 17, also located in the Appendix.

To analyze the behavior of $Ai[\zeta(y)]$ and $Bi[\zeta(y)]$, let us draw our attention to Fig. 5 and Fig. 6, as shown below:

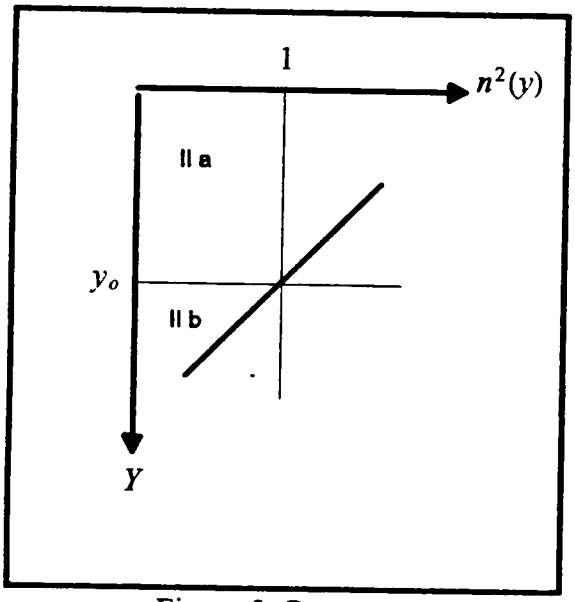

Figure 5. Case one:
$n^2(y)$ with negative gradient.

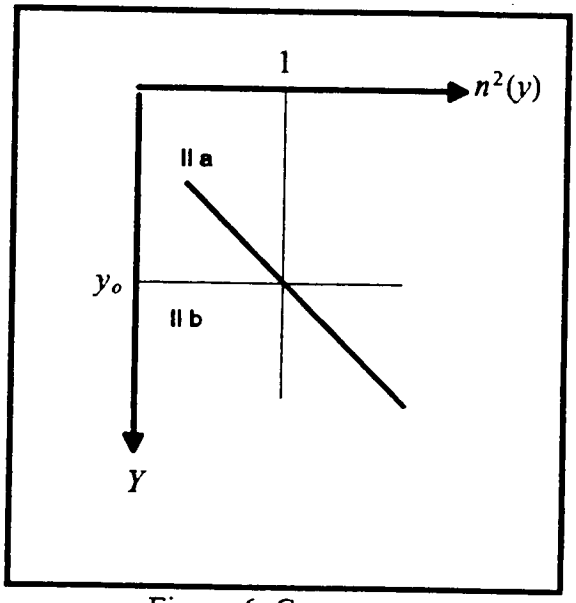

Figure 6. Case two:
$n^2(y)$ with positive gradient.

The free-space solution can be broken into two cases. Case one: $n^2(y)$ has a negative gradient, (see Fig. 5, Fig. 3, Fig. 15 through Fig. 17, and Tables 21 through 23). Case two: $n^2(y)$ has a positive gradient, (see Fig. 6, Fig. 4, Fig. 12 through Fig. 14, and Tables 18 through 20). Also, as can be seen from Fig. 5 and Fig. 6 , each case must be analyzed in two regions, one above the source depth y_0 , and one below the source depth y_0.

First, let us analyze the behavior of the functions $Ai[\zeta(y)]$ and $Bi[\zeta(y)]$ for, Region IIb, Case one. Notice from Fig. 5, that the value of $n^2(y)$ is less than one in this region. Thus, as can be seen from Eq.(2.46), $k_y^2(y)$ will take on negative values. This will result in values of $\zeta(y)$ taking on positive values [see Eq. (2.45)]. Therefore, in Region IIb, Case one we should use the function $Ai[\zeta(y)]$ to ensure a bounded solution since

$$Ai[\zeta(y)] \text{ ------> } 0 \qquad \text{as } \zeta(y) \text{ ------> } +\infty$$

and

$$Bi[\zeta(y)] \text{ ------> } +\infty \qquad \text{as } \zeta(y) \text{ ------> } +\infty.$$

Following a similar argument for Region IIa, Case two we should only use the function $Ai[\zeta(y)]$. Thus, by discarding the Bairy function in Region IIb, Case one and Region IIa, Case two we have ensured that our solution will remain bounded above and below the source as $\zeta(y)$ approaches positive infinity.

Second, for Region IIa, Case one and Region IIb, Case two the value of $n^2(y)$ is greater than one. Thus $k_y^2(y)$ will take on positive values, which leads to negative values for $\zeta(y)$. Therefore, both $Ai[\zeta(y)]$ and $Bi[\zeta(y)]$ should be used in Region IIa, Case one and Region IIb, Case two since both the Airy and Bairy functions are well behaved for negative arguments. The asymptotic forms of the Airy and Bairy functions are defined as follows, [Ref. 4, Chapter 7]

$$Ai[\zeta(y)] = \frac{1}{\sqrt{\pi}}[-\zeta(y)]^{\frac{-1}{4}} \sin[\tfrac{2}{3}[-\zeta(y)]^{\frac{3}{2}} + \tfrac{\pi}{4}] \qquad -\zeta(y) \text{ ---> } +\infty, \qquad (2.47)$$

and

$$Bi[\zeta(y)] = \frac{1}{\sqrt{\pi}}[-\zeta(y)^{\frac{-1}{4}} \cos[\tfrac{2}{3}[-\zeta(y)]^{\frac{3}{2}} + \frac{\pi}{4}] \qquad -\zeta(y) \text{ ---> } +\infty. \qquad (2.48)$$

Thus, to determine the general solution of the inhomogeneous depth equation we must ensure the solution is bounded in Region IIb, Case one and Region IIa, Case two, i.e., $D = 0$ (Case one), see Eq.(2.42) and $B = 0$ (Case two), see Eq.(2.41). Next, we must ensure the solution is in the form of a propagating wave in Region IIa, Case one and Region IIb, Case two, i.e., $A = B_y$ and $a = B/A$ (Case one), see Eq.(2.41), and $C = B_y$ and $b = D/C$ (Case two), see Eq.(2.42). In summary, we have the following forms for the free-space propagation solutions for each case based on Eq.(2.41) and Eq.(2.42):

Case one:

$$\Phi_{f2a}(k_r, y) = B_y\,[Ai[\zeta(y)] + aBi[\zeta(y)]] \qquad \text{for } y \le y_0 \qquad (2.49)$$

$$\Phi_{f2b}(k_r, y) = A_y\,[Ai[\zeta(y)]] \qquad \text{for } y \ge y_0 \qquad (2.50)$$

Case two:

$$\Phi_{f2a}(k_r, y) = A_y\,[Ai[\zeta(y)]] \qquad \text{for } y \le y_0 \qquad (2.51)$$

$$\Phi_{f2b}(k_r, y) = B_y\,[Ai[\zeta(y)] + bBi[\zeta(y)]] \qquad \text{for } y \ge y_0 \qquad (2.52)$$

where A_y and B_y are arbitrary constants and a and b are known constants to be discussed later. Thus, for each case, we have two equations and two unknowns.

To solve for the two unknown constants, we apply the boundary conditions of continuity of acoustic pressure and a discontinuity in the y component of the acoustic fluid velocity vector at the source depth y_0:

1. continuity of acoustic pressure:

$$\Phi_{f2b}(k_r, y_0) - \Phi_{f2a}(k_r, y_0) = 0 \qquad (2.53)$$

2. discontinuity in the y component of the acoustic fluid velocity vector:

$$\frac{d}{dy}\Phi_{f2b}(k_r, y_0) - \frac{d}{dy}\Phi_{f2a}(k_r, y_0) = d \qquad (2.54)$$

where $d = \frac{1}{2\pi}$ is the finite discontinuity, [Ref. 2, Appendix 3C].

CASE ONE:

Substituting Eq.(2.49) and Eq.(2.50) into Eq.(2.53) yields

$$A_y Ai[\zeta(y_0)] - B_y[Ai[\zeta(y_0)] + aBi[\zeta(y_0)]] = 0, \tag{2.55}$$

and upon solving for A_y we obtain

$$A_y = B_y \frac{[Ai[\zeta(y_0)] + aBi[\zeta(y_0)]]}{Ai[\zeta(y_0)]}. \tag{2.56}$$

Substituting Eq.(2.49) and Eq.(2.50) into Eq(2.54) yields

$$-(\alpha_1)^{\frac{1}{3}} A_y Ai'[\zeta(y_0)] - (-)(\alpha_1)^{\frac{1}{3}} B_y[Ai'[\zeta(y_0)] + aBi'[\zeta(y_0)]] = d, \tag{2.57}$$

and upon substituting Eq.(2.56) into Eq.(2.57) and rearranging terms, we obtain

$$\frac{aB_y}{Ai[\zeta(y_0)]}[Bi[\zeta(y_0)]Ai'[\zeta(y_0)] - Ai[\zeta(y_0)]Bi'[\zeta(y_0)]] = -\frac{d}{(\alpha_1)^{\frac{1}{3}}}. \tag{2.58}$$

Since, see [Ref. 1, Chapter 4]

$$Bi[\zeta(y_0)]Ai'[\zeta(y_0)] - Ai[\zeta(y_0)]Bi'[\zeta(y_0)] = -\frac{1}{\pi} \tag{2.59}$$

which is known as the Wronskian of the Airy and Bairy functions, substituting Eq.(2.59) into Eq.(2.58) and solving for B_y yields

$$B_y = \frac{\pi d}{a(\alpha_1)^{\frac{1}{3}}} Ai[\zeta(y_0)]. \tag{2.60}$$

Substituting Eq.(2.60) into Eq.(2.56):

$$A_y = \frac{\pi d}{a(\alpha_1)^{\frac{1}{3}}}[Ai[\zeta(y_0)] + aBi[\zeta(y_0)]]. \tag{2.61}$$

CASE TWO:

Substituting Eq.(2.51) and Eq.(2.52) into Eq.(2.53) yields

$$B_y[Ai[\zeta(y_0)] + bBi[\zeta(y_0)]] - A_y Ai[\zeta(y_0)] = 0, \tag{2.62}$$

and upon solving for A_y, we obtain

$$A_y = B_y \frac{[Ai[\zeta(y_0)] + bBi[\zeta(y_0)]]}{Ai[\zeta(y_0)]}. \tag{2.63}$$

Substituting Eq.(2.51) and Eq.(2.52) into Eq.(2.54) yields

$$-(\alpha_1)^{\frac{1}{3}} B_y[A_i'[\zeta(y_0)] + bB_i'[\zeta(y_0)]] - (-)(\alpha_1)^{\frac{1}{3}} A_y A_i'[\zeta(y_0)] = d, \tag{2.64}$$

and upon substituting Eq.(2.63) into Eq.(2.64) and rearranging terms, we obtain

$$\frac{bB_y}{Ai[\zeta(y_0)]}[Ai[\zeta(y_0)]Bi'[\zeta(y_0)] - Bi[\zeta(y_0)]Ai'[\zeta(y_0)]] = -\frac{d}{(\alpha_1)^{\frac{1}{3}}}. \tag{2.65}$$

Since

$$Ai[\zeta(y_0)]B\hat{i}[\zeta(y_0)] - Bi[\zeta(y_0)]Ai'[\zeta(y_0)] = \frac{1}{\pi}, \tag{2.66}$$

substituting Eq.(2.66) into Eq.(2.65) and solving for B_y yields

$$B_y = -\frac{\pi d}{b(\alpha_1)^{\frac{1}{3}}} Ai[\zeta(y_0)]. \tag{2.67}$$

Substituting Eq.(2.67) into Eq.(2.63) yields

$$A_y = -\frac{\pi d}{b(\alpha_1)^{\frac{1}{3}}}[A_i[\zeta(y_0)] + bB_i[\zeta(y_0)]]. \tag{2.68}$$

Values for the constants a and b must be determined before we have a complete solution. To determine the value of a, recall Eq.(2.49) and Eq.(2.60). Substituting Eq.(2.60) into Eq.(2.49) and rearranging terms yields

$$\Phi_{f2a}(k_r,y) = \frac{\pi d A_i[\zeta(y_0)]}{(\alpha_1)^{\frac{1}{3}}}\left[\frac{1}{a}A_i[\zeta(y)] + B_i[\zeta(y)]\right],\ y \le y_0\,. \tag{2.69}$$

Note that (see Tables 21 through 23, located in the Appendix) as $y \to -\infty$, $\zeta(y) \to -\infty$. Recall the asymptotic expansions of $Ai[\zeta(y)]$ and $Bi[\zeta(y)]$:

$$Ai[\zeta(y)] = \frac{1}{\sqrt{\pi}}[-\zeta(y)]^{\frac{-1}{4}}\sin[\tfrac{2}{3}[-\zeta(y)]^{\frac{3}{2}} + \tfrac{\pi}{4}], \qquad -\zeta(y) \dashrightarrow +\infty \tag{2.70}$$

and

$$Bi[\zeta(y)] = \frac{1}{\sqrt{\pi}}[-\zeta(y)]^{\frac{-1}{4}}\cos[\tfrac{2}{3}[-\zeta(y)]^{\frac{3}{2}} + \tfrac{\pi}{4}], \qquad -\zeta(y) \dashrightarrow +\infty. \tag{2.71}$$

Therefore, substituting Eq.(2.70) and Eq.(2.71) into Eq.(2.69) yields

$$\Phi_{f2a}(k_r,y) = \frac{\pi d A_i[\zeta(y_0)]}{\sqrt{\pi}\,(\alpha_1)^{\frac{1}{3}}}[-\zeta(y)]^{\frac{-1}{4}}\left[\tfrac{1}{a}\sin(\tfrac{2}{3}[-\zeta(y)]^{\frac{3}{2}} + \tfrac{\pi}{4}) + \cos(\tfrac{2}{3}[-\zeta(y)]^{\frac{3}{2}} + \tfrac{\pi}{4})\right]. \tag{2.72}$$

Since this derivation corresponds to a time-harmonic solution with time dependence given by $exp(+j2\pi ft)$, in order to get $\Phi_{f2a}(k_r, y)$ into the form of a wave traveling in the positive $-\zeta(y)$ direction, we must choose $a = +j$ since

$$\exp(-j[-\zeta(y)]) = \cos([-\zeta(y)]) - j\sin([-\zeta(y)]). \tag{2.73}$$

To determine the value of b, we follow a similar logic. Substituting Eq.(2.67) into Eq.(2.52) and rearranging terms yields

$$\Phi_{f2b}(k_r,y) = -\frac{\pi d Ai\zeta(y_0)}{(\alpha_1)^{\frac{1}{3}}}\left[\tfrac{1}{b}Ai[\zeta(y)] + Bi[\zeta(y)]\right], \quad y \geq y_0 . \tag{2.74}$$

Note that (see Tables 18 through 20, located in the Appendix) as $y \to +\infty$, $\zeta(y) \to -\infty$. Using the same logic as before, since $-\zeta(y) \dashrightarrow +\infty$, we must pick $b = +j$ to ensure the correct form of Eq.(2.74).

In summary, we have the following formulas:

CASE ONE:

$$\Phi_{f2a}(k_r,y) = \frac{\pi d Ai[\zeta(y_0)]}{(+j)(\alpha_1)^{\frac{1}{3}}}\{Ai[\zeta(y)] + jBi[\zeta(y)]\}, y \leq y_0 \tag{2.75}$$

and

$$\Phi_{f2b}(k_r,y) = \frac{\pi d\{Ai[\zeta(y_0)] + jBi[\zeta(y_0)]\}}{(+j)(\alpha_1)^{\frac{1}{3}}}Ai[\zeta(y)], y > y_0 \tag{2.76}$$

CASE TWO:

$$\Phi_{f2a}(k_r,y) = -\frac{\pi d\{Ai[\zeta(y_0)] + jBi[\zeta(y_0)]\}}{(+j)(\alpha_1)^{\frac{1}{3}}}Ai[\zeta(y)], y \leq y_0 \tag{2.77}$$

and

$$\Phi_{f2b}(k_r,y) = -\frac{\pi d Ai[\zeta(y_0)]}{(+j)(\alpha_1)^{\frac{1}{3}}}\{Ai[\zeta(y)] + jBi[\zeta(y)]\}, y > y_0 \tag{2.78}$$

Recall that $d = \frac{1}{2\pi}$.

Now that a solution for $\Phi_f(k_r, y)$ has been derived, all that is left to determine the velocity potential is to insert $\Phi_f(k_r, y)$ into Eq.(2.3) and integrate. It is interesting to note, as described in, [Ref. 2, Chapter 9], that:

$$\Phi_f(k_r, y) = H_m(f, f_r, y\,; y_o) \tag{2.79}$$

where $H_m(f, f_r, y\,; y_o)$ is the time-invariant, space-variant ocean medium transfer function. Thus, as described in the Introduction of this thesis, Eq.(2.75) through Eq.(2.78) will be added to the already existing library of ocean medium transfer functions in the program LSVOCN. With this derivation and new transfer function, we can compare the results from LSVOCN to the RRA algorithm to determine the accuracy of the RRA algorithm.

III. COMPARISON OF THE "AIRY FUNCTION" SOLUTION (MAGNITUDE AND PHASE) WITH THE RRA ALGORITHM'S SOLUTION

A. THE TIME-HARMONIC FREE-SPACE GREEN'S FUNCTION AND NUMERICAL ANALYSIS TECHNIQUES

1. The Time-harmonic Free-Space Green's Function for a Homogeneous Ocean Medium

Once the solution to the inhomogeneous Helmholtz equation for a free-space propagation problem with the square of the index of refraction a linear function of depth had been derived, the solution was converted to FORTRAN computer code and added to the computer program LSVOCN as a new ocean medium transfer function. LSVOCN will accept as primary inputs:

1. Sound-speed at the ocean surface and source, in meters/second.
2. Receiver depth and horizontal range relative to the source, in meters.
3. Frequency the source will operate, in Hertz.

The output of LSVOCN is either the velocity potential (magnitude and phase) or the acoustic pressure (magnitude and phase) at a specified receiver location. To test the RRA Algorithm, the depth and horizontal range coordinates of selected points along a ray path, propagated by the RRA Algorithm, will be input into LSVOCN as receiver coordinates. The calculated acoustic pressures (magnitude and phase) from LSVOCN corresponding to these selected points, will be compared with the calculated acoustic pressures (magnitude and phase) from the RRA Algorithm.

Before beginning the testing process, we needed to ensure that both the theoretical solution and FORTRAN computer code were correct. In order to perform this validation, test cases were developed for which theoretical values of the velocity potential could be calculated and compared with the predicted values found using LSVOCN. The time-harmonic free-space Green's function which corresponds to a spherical sound source operating in the monopole mode of vibration in a homogeneous ocean medium, was selected as the basis for these test cases.

As shown in [Ref. 2, Chapter 4], the velocity potential of the acoustic field produced by a spherical sound source in the monopole mode of vibration operating in an unbounded, homogeneous medium is given by

$$\varphi_f(R,\theta,\psi) = S_0 g_f(\underline{r}|\underline{0}) \frac{\exp(+jka)}{1+jka}, \quad R \geq a, \tag{3.1}$$

where S_0 is the source strength (volume flow rate) in m^3/s,

$$g_f(\underline{r}|\underline{0}) = -\frac{\exp(-jkR)}{4\pi R} \tag{3.2}$$

is the time-harmonic free-space Green's function ($\exp(j\omega t)$ factor suppressed) and R is the spherical range between source and receiver. In the limit as $a \to 0$ (modeling a point source) Eq.(3.1) becomes

$$\varphi_f(R,\theta,\psi) = S_0 g_f(\underline{r}|\underline{0}) = -S_0 \frac{\exp(-jkR)}{4\pi R}, \quad R > 0. \tag{3.3}$$

Using Eq.(3.3), theoretical values for the magnitude and phase of an acoustic field at a receiver in an unbounded, homogeneous ocean medium located R meters from a point source can easily be calculated. Although these values are valid only for the homogeneous case, as the modeled ocean medium that LSVOCN uses becomes more homogeneous, then the calculated velocity potential (magnitude and phase) from LSVOCN should approach the predicted values calculated by Eq.(3.3). The theoretical magnitude of the velocity potential calculated by Eq.(3.3) is given by

$$|\varphi_f| = \frac{S_o}{4\pi R}. \tag{3.4}$$

The theoretical phase of the velocity potential calculated by Eq.(3.3) is given by

$$\angle\varphi_f = \pi\left(\pm 1 - \frac{2fR}{c}\right) \tag{3.5}$$

where f is the frequency at which the source operates, R is the spherical range between the source and receiver, and c is the speed of sound. In order to test the Airy function solution and the corresponding FORTRAN computer code in LSVOCN, Eq.(3.4) and Eq.(3.5) were used in three different Green's function test cases, defined as follows:

1. With the receiver and source depth equal, and with the receiver one meter from the source, vary the speed of sound at the source so that it approaches the speed of sound at the surface.

2. With the receiver and source depth equal, and the source sound-speed constant, vary the horizontal range between the source and receiver.

3. With the source sound-speed constant, vary the receiver depth.

Each of these test cases will be covered in detail in Section B of this chapter.

2. Numerical Analysis Techniques

Recall from Eq.(2.3) that

$$\varphi_f(r,y) = H^{-1}\{\Phi_f(k_r,y)\} = \int_0^\infty \Phi_f(k_r,y) J_0(k_r r) k_r dk_r. \tag{3.6}$$

In order to calculate the exact "Airy function" solution at a given receiver depth and horizontal range, the integral in Eq.(3.6) must be computed. As we discovered, this integral is difficult to evaluate numerically. The integrand in Eq.(3.6) is oscillatory due to the Bessel function, when negative arguments of the Airy and Bairy functions are involved. Numerous overflow and underflow errors were generated when Eq.(3.6) was calculated numerically with the computer. To eliminate overflow errors, the exponentially scaled versions of the Airy and Bairy functions were used. The following example illustrates the method of using the exponentially scaled Airy and Bairy functions to eliminate overflow errors.

In order to solve Eq.(2.75) or Eq.(2.78) for the case of propagating waves, it is necessary to multiply the Airy and Bairy functions together. Although the argument of these functions, $\zeta(y)$, is more likely to take on negative values in regions IIa, Case one

and region IIb, Case two, once the propagating waves turn evanescent, the value for $\zeta(y)$ is forced to take on positive values which cause the Bairy function to blow up, leading to overflow errors. By experimentation it was discovered that the computer could handle values of $\zeta(y)$ up to positive forty, without generating overflow errors. However, to include most of the evanescent waves, $\zeta(y)$ must be allowed to take on much larger positive values, which requires the use of the exponentially scaled Airy and Bairy functions:

1.DAI(x), DBI(x) -- double-precision IMSL Airy and Bairy functions.

2.DAIE(x), DBIE(x) -- double-precision IMSL exponentially scaled and Bairy functions.

where

$$DAIE(x) = DAI(x) \times \exp(\tfrac{2}{3}x^{\frac{3}{2}}) \tag{3.7}$$

and

$$DBIE(x) = DBI(x) \times \exp(-\tfrac{2}{3}x^{\frac{3}{2}}). \tag{3.8}$$

Therefore when multiplying $Ai[\zeta(y)]$ and $Bi[\zeta(y)]$, first form the difference term:

$$DIFF = \tfrac{2}{3}\left[\zeta(y_o)^{\frac{2}{3}} - \zeta(y)^{\frac{2}{3}}\right]. \tag{3.9}$$

Then perform the required multiplication as follows:

$$A_i[\zeta(y_o)] \times B_i[\zeta(y)] = \exp(-DIFF) \times DAIE[\zeta(y_o)] \times DBIE[\zeta(y)]\,. \tag{3.10}$$

This method of multiplying the Airy and Bairy functions together allows for much larger values of $\zeta(y)$ to be used. Thus most of the evanescent waves could be included. Underflow errors did not offer the same problems that overflow errors caused since the machine handled underflow errors without termination of the computer program LSVOCN. However, small inaccuracies from underflow errors had to be expected.

These same techniques can be used to solve Eq.(2.76) and Eq.(2.77). Overflow errors were not a problem for these two equations since the Bairy function was not part of the solution. Graphical presentations of the Airy and Bairy functions are included in Figures 7 and 8. Tabulated values of the Airy and Bairy functions, the exponentially scaled Airy and Bairy functions, and EDAIE(x) and EDBIE(x) are included in Table 1. The functions EDAIE(x) and EDBIE(x) are the exponentially scaled Airy and Bairy functions multiplied by the appropriate exponential factor that eliminates the exponential scaling. These values were also tabulated to ensure that the numerical method represented by Eq.(3.9) and Eq.(3.10) would produce the same values as if the exponentially scaled functions were not used. This can be observed in Table 1 by noticing that DAI(X) = EDAIE(X) and that DBI(X) = EDBIE(X).

To solve for the velocity potential, Eq.(3.6) must theoretically be integrated from zero to infinity. In practice, the upper limit of integration need not be infinity, but rather a sufficiently large number so that the integrand becomes negligible in value, in other words, all significant evanesent waves are included. A method was developed to automatically generate the upper limit of integration. This method will be discussed next.

We begin with Eq.(2.45), rewritten here for convenience:

$$\zeta(y) = -(\alpha_1)^{-\frac{2}{3}} k_y^2(y). \tag{3.11}$$

Equation (3.11) can rewritten as

$$\zeta(y) = -\frac{1}{\sqrt[3]{(a_1 k_0^2)^2}}[k^2(y) - k_r^2], \tag{3.12}$$

and upon rearranging terms and solving for k_r, we obtain

$$k_r = +\sqrt{k^2(y) + \left[\sqrt[3]{(a_1 k_0^2)^2}\right]\zeta(y)}\,. \tag{3.13}$$

X	DAIE(X)
0.0E+00	0.355028E+00
0.1E+02	0.158124E+00
0.1E+03	0.891969E-01
0.1E+04	0.501642E-01
0.1E+05	0.282095E-01
0.1E+06	0.158634E-01
0.1E+07	0.892062E-02
0.1E+08	0.501643E-02
0.1E+09	0.282095E-02
0.1E+10	0.158634E-02
0.1E+11	0.892062E-03
0.1E+12	0.501643E-03
0.1E+13	0.282095E-03
0.1E+14	0.158634E-03
0.1E+15	0.892062E-04
0.1E+16	0.501643E-04
0.1E+17	0.282095E-04
0.1E+18	0.158633E-04
0.1E+19	0.892062E-05
0.1E+20	0.501643E-05
0.1E+21	0.282095E-05
0.1E+22	0.158634E-05
0.1E+23	0.892062E-06
0.1E+24	0.501643E-06
0.1E+25	0.282095E-06
0.1E+26	0.158634E-06
0.1E+27	0.892062E-07
0.1E+28	0.501643E-07
0.1E+29	0.282095E-07
0.1E+30	0.158634E-07
0.1E+31	0.892062E-08
0.1E+32	0.501643E-08
0.1E+33	0.282095E-08
0.1E+34	0.158634E-08
0.1E+35	0.892062E-09
0.1E+36	0.501643E-09
0.1E+37	0.282095E-09
0.1E+38	0.158634E-09
0.1E+39	0.892062E-10
0.1E+40	0.501643E-10
0.1E+41	0.282095E-10
0.1E+42	0.158634E-10

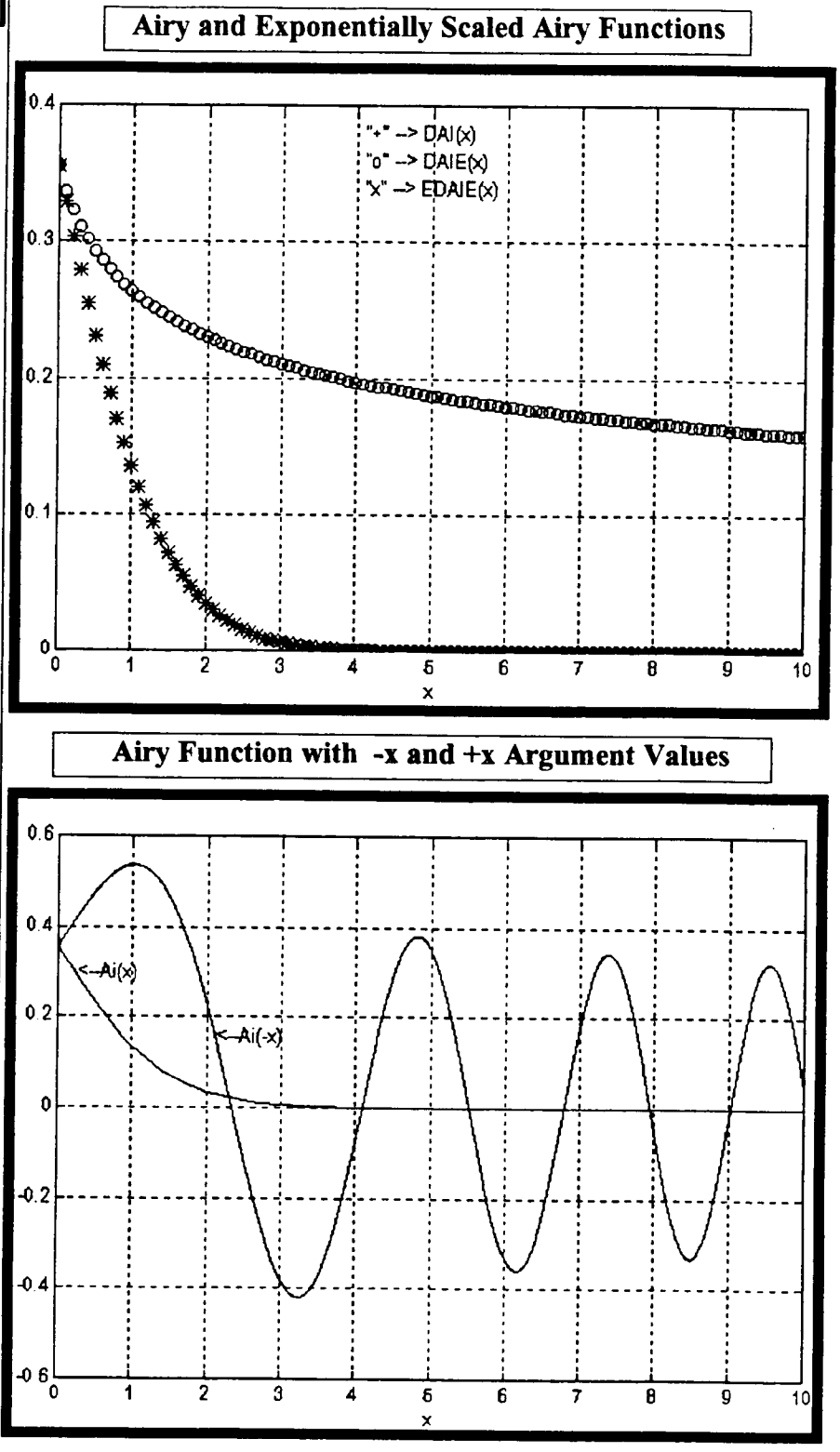

Figure 7. Tabulated values of DAIE(x) and plots of DAI(x), DAI(-x), DAIE(x), and EDAIE(x).

X	DBIE(X)
0.0E+00	0.614927E+00
0.1E+02	0.318340E+00
0.1E+03	0.178431E+00
0.1E+04	0.100329E+00
0.1E+05	0.564190E-01
0.1E+06	0.317267E-01
0.1E+07	0.178412E-01
0.1E+08	0.100329E-01
0.1E+09	0.564189E-02
0.1E+10	0.317267E-02
0.1E+11	0.178412E-02
0.1E+12	0.100329E-02
0.1E+13	0.564189E-03
0.1E+14	0.317267E-03
0.1E+15	0.178412E-03
0.1E+16	0.100329E-03
0.1E+17	0.564190E-04
0.1E+18	0.317267E-04
0.1E+19	0.178412E-04
0.1E+20	0.100329E-04
0.1E+21	0.564190E-05
0.1E+22	0.317267E-05
0.1E+23	0.178412E-05
0.1E+24	0.100329E-05
0.1E+25	0.564190E-06
0.1E+26	0.317267E-06
0.1E+27	0.178412E-06
0.1E+28	0.100329E-06
0.1E+29	0.564190E-07
0.1E+30	0.317267E-07
0.1E+31	0.178412E-07
0.1E+32	0.100329E-07
0.1E+33	0.564189E-08
0.1E+34	0.317267E-08
0.1E+35	0.178412E-08
0.1E+36	0.100329E-08
0.1E+37	0.564189E-09
0.1E+38	0.317267E-09
0.1E+39	0.178412E-09
0.1E+40	0.100329E-09
0.1E+41	0.564190E-10
0.1E+42	0.317267E-10

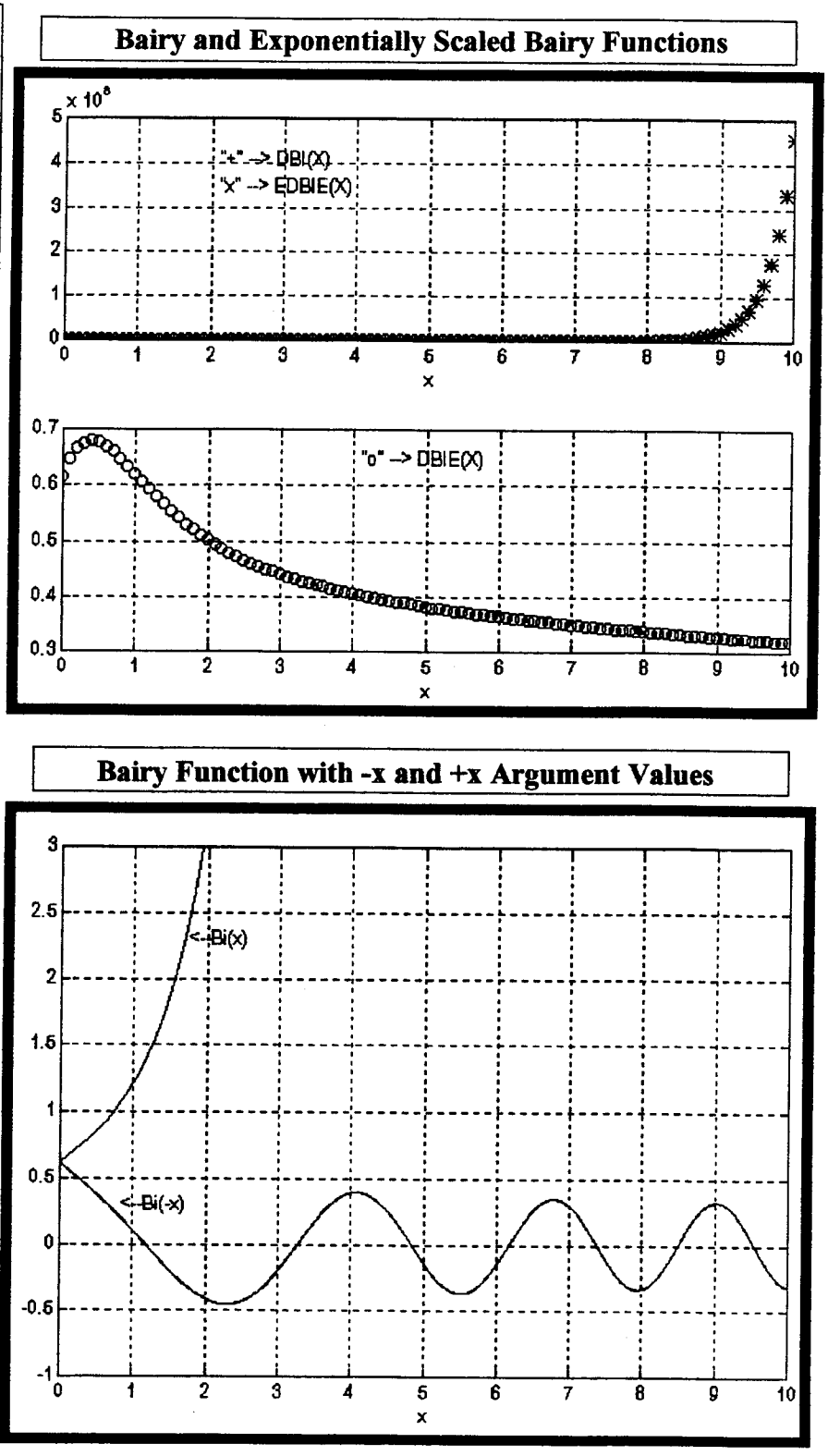

Figure 8. Tabulated values of DBIE(x) and plots of DBI(x), DBI(-x), DBIE(x), and EDBIE(x).

X	DAI(X)	DAIE(X)	EDAIE(X)
0.00	0.355028E+00	0.355028E+00	0.355028E+00
0.10	0.329203E+00	0.336217E+00	0.329203E+00
0.20	0.303703E+00	0.322363E+00	0.303703E+00
0.30	0.278806E+00	0.311084E+00	0.278806E+00
0.40	0.254742E+00	0.301541E+00	0.254742E+00
0.50	0.231694E+00	0.293277E+00	0.231694E+00
0.60	0.209800E+00	0.286000E+00	0.209800E+00
0.70	0.189162E+00	0.279513E+00	0.189162E+00
0.80	0.169846E+00	0.273670E+00	0.169846E+00
0.90	0.151887E+00	0.268364E+00	0.151887E+00
1.00	0.135292E+00	0.263514E+00	0.135292E+00
1.10	0.120049E+00	0.259052E+00	0.120049E+00
1.20	0.106126E+00	0.254928E+00	0.106126E+00
1.30	0.934746E-01	0.251098E+00	0.934746E-01
1.40	0.820380E-01	0.247527E+00	0.820380E-01
1.50	0.717494E-01	0.244185E+00	0.717495E-01
1.60	0.625369E-01	0.241048E+00	0.625369E-01
1.70	0.543248E-01	0.238094E+00	0.543248E-01
1.80	0.470362E-01	0.235306E+00	0.470362E-01
1.90	0.405944E-01	0.232667E+00	0.405944E-01
2.00	0.349241E-01	0.230165E+00	0.349241E-01
2.10	0.299526E-01	0.227786E+00	0.299526E-01
2.20	0.256104E-01	0.225522E+00	0.256104E-01
2.30	0.218320E-01	0.223361E+00	0.218320E-01
2.40	0.185561E-01	0.221297E+00	0.185561E-01
2.50	0.157259E-01	0.219322E+00	0.157259E-01
2.60	0.132893E-01	0.217429E+00	0.132893E-01
2.70	0.111985E-01	0.215613E+00	0.111985E-01
2.80	0.941050E-02	0.213868E+00	0.941051E-02
2.90	0.788631E-02	0.212189E+00	0.788631E-02
3.00	0.659114E-02	0.210572E+00	0.659114E-02
3.10	0.549399E-02	0.209013E+00	0.549399E-02
3.20	0.456744E-02	0.207509E+00	0.456744E-02
3.30	0.378729E-02	0.206056E+00	0.378729E-02
3.40	0.313234E-02	0.204651E+00	0.313234E-02
3.50	0.258410E-02	0.203292E+00	0.258410E-02
3.60	0.212648E-02	0.201976E+00	0.212648E-02
3.70	0.174557E-02	0.200700E+00	0.174557E-02
3.80	0.142939E-02	0.199462E+00	0.142939E-02
3.90	0.116765E-02	0.198261E+00	0.116765E-02
4.00	0.951564E-03	0.197095E+00	0.951564E-03
4.10	0.773630E-03	0.195961E+00	0.773629E-03
4.20	0.627496E-03	0.194859E+00	0.627496E-03
4.30	0.507787E-03	0.193786E+00	0.507787E-03
4.40	0.409974E-03	0.192741E+00	0.409974E-03
4.50	0.330250E-03	0.191724E+00	0.330250E-03
4.60	0.265432E-03	0.190732E+00	0.265432E-03
4.70	0.212861E-03	0.189765E+00	0.212861E-03
4.80	0.170326E-03	0.188822E+00	0.170325E-03
4.90	0.135992E-03	0.187901E+00	0.135992E-03
5.00	0.108344E-03	0.187002E+00	0.108344E-03
5.10	0.861324E-04	0.186124E+00	0.861324E-04
5.20	0.683285E-04	0.185265E+00	0.683285E-04
5.30	0.540905E-04	0.184426E+00	0.540905E-04
5.40	0.427299E-04	0.183605E+00	0.427298E-04
5.50	0.336853E-04	0.182802E+00	0.336853E-04
5.60	0.265006E-04	0.182015E+00	0.265006E-04
5.70	0.208058E-04	0.181246E+00	0.208058E-04
5.80	0.163017E-04	0.180491E+00	0.163017E-04
5.90	0.127471E-04	0.179753E+00	0.127471E-04
6.00	0.994769E-05	0.179028E+00	0.994769E-05
6.10	0.774773E-05	0.178318E+00	0.774773E-05
6.20	0.602246E-05	0.177622E+00	0.602246E-05
6.30	0.467226E-05	0.176939E+00	0.467226E-05

X	DBI(X)	DBIE(X)	EDBIE(X)
0.00	0.614927E+00	0.614927E+00	0.614927E+00
0.10	0.659862E+00	0.646096E+00	0.659862E+00
0.20	0.705464E+00	0.664628E+00	0.705464E+00
0.30	0.752486E+00	0.674409E+00	0.752486E+00
0.40	0.801773E+00	0.677338E+00	0.801773E+00
0.50	0.854277E+00	0.674892E+00	0.854277E+00
0.60	0.911063E+00	0.668324E+00	0.911063E+00
0.70	0.973329E+00	0.658708E+00	0.973329E+00
0.80	0.104242E+01	0.646954E+00	0.104242E+01
0.90	0.111987E+01	0.633817E+00	0.111987E+01
1.00	0.120742E+01	0.619912E+00	0.120742E+01
1.10	0.130707E+01	0.605721E+00	0.130707E+01
1.20	0.142113E+01	0.591614E+00	0.142113E+01
1.30	0.155228E+01	0.577859E+00	0.155228E+01
1.40	0.170366E+01	0.564646E+00	0.170366E+01
1.50	0.187894E+01	0.552094E+00	0.187894E+01
1.60	0.208247E+01	0.540272E+00	0.208247E+01
1.70	0.231941E+01	0.529208E+00	0.231941E+01
1.80	0.259587E+01	0.518898E+00	0.259587E+01
1.90	0.291918E+01	0.509320E+00	0.291918E+01
2.00	0.329809E+01	0.500437E+00	0.329809E+01
2.10	0.374315E+01	0.492203E+00	0.374315E+01
2.20	0.426704E+01	0.484567E+00	0.426704E+01
2.30	0.488506E+01	0.477480E+00	0.488506E+01
2.40	0.561577E+01	0.470890E+00	0.561577E+01
2.50	0.648166E+01	0.464750E+00	0.648166E+01
2.60	0.751009E+01	0.459017E+00	0.751009E+01
2.70	0.873439E+01	0.453648E+00	0.873439E+01
2.80	0.101953E+02	0.448608E+00	0.101953E+02
2.90	0.119426E+02	0.443863E+00	0.119426E+02
3.00	0.140373E+02	0.439384E+00	0.140373E+02
3.10	0.165547E+02	0.435146E+00	0.165547E+02
3.20	0.195870E+02	0.431125E+00	0.195870E+02
3.30	0.232483E+02	0.427301E+00	0.232483E+02
3.40	0.276796E+02	0.423657E+00	0.276796E+02
3.50	0.330555E+02	0.420177E+00	0.330555E+02
3.60	0.395927E+02	0.416848E+00	0.395927E+02
3.70	0.475607E+02	0.413656E+00	0.475607E+02
3.80	0.572954E+02	0.410592E+00	0.572954E+02
3.90	0.692160E+02	0.407646E+00	0.692160E+02
4.00	0.838471E+02	0.404809E+00	0.838471E+02
4.10	0.101846E+03	0.402075E+00	0.101846E+03
4.20	0.124038E+03	0.399435E+00	0.124038E+03
4.30	0.151462E+03	0.396884E+00	0.151462E+03
4.40	0.185428E+03	0.394417E+00	0.185428E+03
4.50	0.227588E+03	0.392027E+00	0.227588E+03
4.60	0.280036E+03	0.389712E+00	0.280036E+03
4.70	0.345426E+03	0.387466E+00	0.345426E+03
4.80	0.427126E+03	0.385286E+00	0.427126E+03
4.90	0.529425E+03	0.383168E+00	0.529425E+03
5.00	0.657792E+03	0.381109E+00	0.657792E+03
5.10	0.819209E+03	0.379105E+00	0.819210E+03
5.20	0.102261E+04	0.377155E+00	0.102262E+04
5.30	0.127947E+04	0.375256E+00	0.127947E+04
5.40	0.160448E+04	0.373405E+00	0.160448E+04
5.50	0.201658E+04	0.371600E+00	0.201658E+04
5.60	0.254018E+04	0.369839E+00	0.254018E+04
5.70	0.320680E+04	0.368120E+00	0.320680E+04
5.80	0.405720E+04	0.366441E+00	0.405720E+04
5.90	0.514421E+04	0.364800E+00	0.514422E+04
6.00	0.653645E+04	0.363197E+00	0.653645E+04
6.10	0.832309E+04	0.361629E+00	0.832309E+04
6.20	0.106204E+05	0.360095E+00	0.106204E+05
6.30	0.135799E+05	0.358593E+00	0.135800E+05

Table 1. Tabulated values for DAI(x), DAIE(x), EDAIE(x), DBI(x), DBIE(x), and EDBIE(x).

Before the exponentially scaled Airy and Bairy functions were used, the largest positive value of the argument for the Bairy function that could be evaluated by the computer without causing overflow errors was $\zeta(y) = \zeta_{max} = 40$. By using the exponentially scaled Airy and Bairy functions, it was discovered that ζ_{max} could take on extremely large values, for example, $\zeta_{max} = 10^{12} - 10^{16}$. Substituting ζ_{max} into Eq.(3.13) for $\zeta(y)$ resulted in the following equation for the upper limit of integration.

$$k_{r\max} = +\sqrt{k^2(y) + \left[\sqrt[3]{(a_1 k_0^2)^2}\right]\zeta_{\max}} \tag{3.14}$$

Therefore, the upper limit of integration used in Eq.(3.6) could automatically be adjusted to the maximum possible value regardless of the frequency selected. However, due to the oscillatory nature of the Bessel function and the dependence of its argument on k_r and r, the integrand of Eq.(3.6) becomes increasingly difficult to integrate numerically as k_r increases (for a fixed r), because as the wave number of the Bessel function increases, the function becomes more highly oscillatory. To ensure accurate results from the computer code, the region of integration had to be divided into subintervals in performing the numerical integration. This method enabled LSVOCN to calculate increasingly many evanescent waves providing more accurate results.

B. COMPARISON OF LSVOCN WITH THE TIME-HARMONIC FREE-SPACE GREEN'S FUNCTION FOR A HOMOGENOUS OCEAN MEDIUM

1. Green's Function Test Case One - Vary the Source Sound-Speed

The first test case involved varying the source, operating at frequencies of 1000 Hz, 250 Hz, and 50 Hz, sound-speed while maintaining the surface sound-speed fixed, using both positive and negative gradients for the square of the index of refraction. Each case had an initial source sound-speed of 1515 m/s for the negative gradient of the square of the index of refraction, and 1485 m/s for the positive gradient case. The source and receiver depths were held constant at 150 meters, with the receiver located one meter

in horizontal range from the source. For each successive run of the test case, the source sound-speed was decreased/increased by a factor of 3 m/s until 1501 m/s and 1499 m/s was reached, respectively, while maintaining the surface sound-speed constant at 1500 m/s. Thus, the source sound-speed was never allowed to take on a value of 1500 m/s, ensuring that the Airy function solution of LSVOCN, which assumed a sound-speed profile where the square of the index of refraction was a linear function of depth, would remain valid while at the same time forcing the modeled ocean medium to become more homogeneous. If the derived Airy function solution and the corresponding computer code in LSVOCN were correct, then as the source sound-speed approached the surface sound-speed, the velocity potential (magnitude and phase) values calculated by LSVOCN would converge approximately to the velocity potential (magnitude and phase) values predicted by Eq.(3.4) and (3.5), respectively. Because we were making calculations at the source depth, the *DIFF* term given by Eq.(3.9) was equal to zero, which made the exp(-*DIFF*) term in Eq.(3.10) equal to one. This condition caused the oscillations of the integrand in Eq.(3.6) to decay very slowly, thus requiring longer integration causing an increase in CPU time. A summary of these test cases is included as Tables 2 through 7.

The Delta's and percentage differences included in Tables 2 through 7 were calculated as follows:

1. Delta magnitude = LSVOCN magnitude - Green's function magnitude
2. Delta phase = LSVOCN phase - Green's function phase

3. $\%\ \text{Difference magnitude} = \frac{\text{LSVOCN mag - Green's function mag}}{\text{Green's function mag}} \times 100\%$

4. $\%\ \text{Difference phase} = \frac{\text{LSVOCN phase - Green's function phase}}{\text{Green's function phase}} \times 100\%$

The data in Tables 2 through 7, show that as the source sound-speed approaches the surface sound-speed, making the modeled ocean medium more homogeneous, the calculated velocity potential (magnitude and phase) values from LSVOCN approach the velocity potential (magnitude and phase) values predicted by the Green's function - our first validation.

SOURCE FREQUENCY = 1000Hz SOURCE DEPTH = RECEIVER DEPTH = 150 METERS SURFACE SOUND-SPEED = 1500 m/s								
Sound Speed Source m/s	**Magnitude Green's Func m^2/s**	**Phase Green's Func Deg.**	**Magnitude LSVOCN m^2/s**	**Phase LSVOCN Deg.**	**Delta Magnitude m^2/s**	**Delta Phase Deg.**	**% Difference Magnitude**	**% Difference Phase**
1515	0.0795775	302.37624	0.0787327	302.557	-0.0008448	0.18076	-1.0616066	0.0597798
1512	0.0795775	301.90476	0.0787842	302.059	-0.0007933	0.15424	-0.9968898	0.051089
1509	0.0795775	301.43141	0.0788504	301.559	-0.0007271	0.12759	-0.9137005	0.042328
1506	0.0795775	300.95618	0.0789223	301.039	-0.0006552	0.08282	-0.8233483	0.027519
1503	0.0795775	300.47904	0.0790248	300.502	-0.0005527	0.02296	-0.6945431	0.0076411
1501	0.0795775	300.15989	0.0791721	300.148	-0.0004054	-0.01189	-0.5094405	-0.0039612

Table 2. Comparison of Green's Function with LSVOCN for Test Case 1 (Vary the Source Sound-Speed) - $n^2(y)$ with Negative Gradient.

SOURCE FREQUENCY = 250Hz SOURCE DEPTH = RECEIVER DEPTH = 150 METERS SURFACE SOUND-SPEED = 1500 m/s								
Sound Speed Source m/s	**Magnitude Green's Func m^2/s**	**Phase Green's Func Deg.**	**Magnitude LSVOCN m^2/s**	**Phase LSVOCN Deg.**	**Delta Magnitude m^2/s**	**Delta Phase Deg.**	**% Difference Magnitude**	**% Difference Phase**
1515	0.0795775	120.59406	0.0791376	120.992	-0.0004399	0.39794	-0.5527944	0.3299831
1512	0.0795775	120.47619	0.0791609	120.83	-0.0004166	0.35381	-0.5235148	0.2936763
1509	0.0795775	120.35785	0.0792156	120.704	-0.0003619	0.34615	-0.4547768	0.2876007
1506	0.0795775	120.23904	0.07923	120.502	-0.0003475	0.26296	-0.4366812	0.2186977
1503	0.0795775	120.11976	0.0793777	120.422	-0.0001998	0.30224	-0.251076	0.2516156
1501	0.0795775	120.03997	0.0794475	120.263	-0.00013	0.22303	-0.1633628	0.1857964

Table 3. Comparison of Green's Function with LSVOCN for Test Case 1 (Vary the Source Sound-Speed) - $n^2(y)$ with Negative Gradient.

SOURCE FREQUENCY = 50Hz SOURCE DEPTH = RECEIVER DEPTH = 150 METERS SURFACE SOUND-SPEED = 1500 m/s								
Sound Speed Source m/s	**Magnitude Green's Func m^2/s**	**Phase Green's Func Deg.**	**Magnitude LSVOCN m^2/s**	**Phase LSVOCN Deg.**	**Delta Magnitude m^2/s**	**Delta Phase Deg.**	**%Difference Magnitude**	**% Difference Phase**
1515	0.0795775	168.11881	0.079782	168.366	0.0002045	0.24719	0.2569822	0.1470329
1512	0.0795775	168.09524	0.0797383	168.322	0.0001608	0.22676	0.2020672	0.1348997
1509	0.0795775	168.07157	0.0797825	168.286	0.000205	0.21443	0.2576105	0.1275826
1506	0.0795775	168.04781	0.079723	168.231	0.0001455	0.18319	0.1828406	0.1090106
1503	0.0795775	168.02395	0.0797083	168.172	0.0001308	0.14805	0.1643681	0.0881124
1501	0.0795775	168.00799	0.0798172	168.133	0.0002397	0.12501	0.3012158	0.0744072

Table 4. Comparison of Green's Function with LSVOCN for Test Case 1 (Vary the Source Sound-Speed) - $n^2(y)$ with Negative Gradient.

SOURCE FREQUENCY = 1000Hz
SOURCE DEPTH = RECEIVER DEPTH = 150 METERS
SURFACE SOUND-SPEED = 1500 m/s

Sound Speed Source m/s	Magnitude Green's Func m^2/s	Phase Green's Func Deg.	Magnitude LSVOCN m^2/s	Phase LSVOCN Deg.	Delta Magnitude m^2/s	Delta Phase Deg.	% Difference Magnitude	% Difference Phase
1485	0.0795775	297.57576	0.0787358	297.709	-0.0008417	0.13324	-1.057711	0.0447752
1488	0.0795775	298.06452	0.0787811	298.174	-0.0007964	0.10948	-1.0007854	0.0367303
1491	0.0795775	298.55131	0.0788484	298.647	-0.0007291	0.09569	-0.9162138	0.0320514
1494	0.0795775	299.03614	0.0789214	299.099	-0.0006561	0.06286	-0.8244793	0.0210209
1497	0.0795775	299.51904	0.079039	299.546	-0.0005385	0.02696	-0.6766988	0.0090011
1499	0.0795775	299.83989	0.079143	299.839	-0.0004345	-0.00089	-0.5460086	-0.0002968

Table 5. Comparison of Green's Function with LSVOCN for Test Case 1 (Vary the Source Sound-Speed) - $n^2(y)$ with Positive Gradient.

SOURCE FREQUENCY = 250Hz
SOURCE DEPTH = RECEIVER DEPTH = 150 METERS
SURFACE SOUND-SPEED = 1500 m/s

Sound Speed Source m/s	Magnitude Green's Func m^2/s	Phase Green's Func Deg.	Magnitude LSVOCN m^2/s	Phase LSVOCN Deg.	Delta Magnitude m^2/s	Delta Phase Deg.	% Difference Magnitude	% Difference Phase
1485	0.0795775	119.39394	0.0791194	119.774	-0.0004581	0.38006	-0.5756652	0.3183244
1488	0.0795775	119.51613	0.0791708	119.885	-0.0004067	0.36887	-0.5110741	0.3086362
1491	0.0795775	119.63783	0.0791928	119.958	-0.0003847	0.32017	-0.4834281	0.267616
1494	0.0795775	119.75904	0.0792593	120.06	-0.0003182	0.30096	-0.3998618	0.2513046
1497	0.0795775	119.87976	0.0793556	120.145	-0.0002219	0.26524	-0.2788477	0.221255
1499	0.0795775	119.95997	0.0794502	120.185	-0.0001273	0.22503	-0.1599698	0.1875876

Table 6. Comparison of Green's Function with LSVOCN for Test Case 1 (Vary the Source Sound-Speed) - $n^2(y)$ with Positive Gradient.

SOURCE FREQUENCY = 50Hz
SOURCE DEPTH = RECEIVER DEPTH = 150 METERS
SURFACE SOUND-SPEED = 1500 m/s

Sound Speed Source m/s	Magnitude Green's Func m^2/s	Phase Green's Func Deg.	Magnitude LSVOCN m^2/s	Phase LSVOCN Deg.	Delta Magnitude m^2/s	Delta Phase Deg.	% Difference Magnitude	% Difference Phase
1485	0.0795775	167.87879	0.0797431	168.123	0.0001656	0.24421	0.208099	0.145468
1488	0.0795775	167.90323	0.0797786	168.138	0.0002011	0.23477	0.2527096	0.1398246
1491	0.0795775	167.92757	0.0797322	168.136	0.0001547	0.20843	0.1944017	0.124119
1494	0.0795775	167.95181	0.0797651	168.142	0.0001876	0.19019	0.235745	0.1132408
1497	0.0795775	167.97595	0.0797772	168.135	0.0001997	0.15905	0.2509503	0.0946862
1499	0.0795775	167.99199	0.0797195	168.103	0.000142	0.11101	0.1784424	0.0660805

Table 7. Comparison of Green's Function with LSVOCN for Test Case 1 (Vary the Source Sound-Speed) - $n^2(y)$ with Positive Gradient.

2. Green's Function Test Case Two - Vary the Horizontal Range

The second test case involved varying the horizontal range while maintaining the source and receiver depths fixed at 150 meters. For this case the surface and source sound-speeds are not varied. If the receiver is fixed at the source depth (150 meters) and the horizontal range is increased, then the magnitude of the velocity potential should decrease by a factor of $1/4\pi R$, independent of frequency, as predicted by Eq.(3.4). Furthermore, it should be observed that the phase varies as predicted by Eq.(3.5):

$$\angle\varphi_f = \pi\left(\pm 1 - \frac{2fR}{c}\right). \tag{3.15}$$

The above observations are reasonable assumptions to make even though the modeled ocean medium is not homogeneous. As long as the receiver is maintained at the same depth as the source, then the sound speed is constant, which simulates a homogeneous ocean medium.

To conduct the second Green's function test case, the receiver depth and source depth are both fixed at 150 meters. The surface sound-speed is fixed at 1500 m/s and the source sound-speed is fixed at 1515 m/s for a negative gradient for the square of the index of refraction, and 1485 m/s for a positive gradient for the square of the index of refraction. Horizontal range values selected were 2.0, 3.0, and 5.0 meters. These values were selected based on the amount of CPU time required to calculate the velocity potential (magnitude and phase) for each selected receiver depth, horizontal range pair. Because we were making calculations at the source depth, the *DIFF* term given by Eq.(3.9) was equal to zero, which made the exp(-*DIFF*) term in Eq.(3.10) equal to one. This condition caused the oscillations of the integrand in Eq.(3.6) to decay very slowly, thus making integration more difficult resulting in more CPU time being required. In addition, as k_r increases (for a fixed r) the zeroth-order Bessel function in Eq.(3.6) oscillates more rapidly, making the numerical integration more difficult. Any calculation requiring more than 60 minutes of CPU time was stopped by the computer. The test case results are summarized in Tables 8 and 9. Calculations that required greater than 60

minutes of CPU time are denoted by: >60 min. The delta's and percentage differences were calculated in the same manner as discussed previously. The data in Tables 8 and 9 show that as the horizontal range increases while maintaining the receiver at the source depth, the velocity potential (magnitude and phase) calculated by LSVOCN behaves according to the Green's function for a free-space homogeneous ocean medium as predicted by Eq.(3.4) and Eq.(3.5) with $S_0 = 1$ - our second validation.

SOURCE DEPTH = RECEIVER DEPTH = 150 METERS
SURFACE SOUND-SPEED = 1500 m/s SOURCE SOUND-SPEED = 1515 m/s

Frequency Hertz	Range meters	Green's Func Magnitude m^2/s	Green's Func Phase Deg.	LSVOCN Magnitude m^2/s	LSVOCN Phase Deg.	Delta Magnitude m^2/s	Delta Phase Deg.	% Difference Magnitude	% Difference Phase
1000	2	0.0397887	64.752475	>60 min	>60 min	N/A	N/A	N/A	N/A
	3	0.0265258	187.12871	>60 min	>60 min	N/A	N/A	N/A	N/A
	5	0.0159155	71.881188	>60 min	>60 min	N/A	N/A	N/A	N/A
250	2	0.0397887	61.188119	0.0395919	61.221	-0.0001968	0.032881	-0.4946128	0.0537376
	3	0.0265258	1.7821782	0.0264635	2.343	-0.0000623	0.5608218	-0.2348657	31.4683346
	5	0.0159155	242.9703	>60 min	>60 min	N/A	N/A	N/A	N/A
50	2	0.0397887	156.23762	0.0397634	156.67	-0.0000253	0.43238	-0.0635859	0.2767451
	3	0.0265258	144.35644	0.0264378	144.937	-0.000088	0.58056	-0.3317525	0.4021712
	5	0.0159155	120.59406	0.0157484	121.152	-0.0001671	0.55794	-1.0499199	0.4626596

Table 8. Comparison of Green's Function with LSVOCN for Test Case 2 (Vary Horizontal Range) - $n^2(y)$ with Negative Gradient.

SOURCE DEPTH = RECEIVER DEPTH = 150 METERS
SURFACE SOUND-SPEED = 1500 m/s SOURCE SOUND-SPEED = 1485 m/s

Frequency Hertz	Range meters	Green's Func Magnitude m^2/s	Green's Func Phase Deg.	LSVOCN Magnitude m^2/s	LSVOCN Phase Deg.	Delta Magnitude m^2/s	Delta Phase Deg.	% Difference Magnitude	% Difference Phase
1000	2	0.0397887	55.151515	>60 min	>60 min	N/A	N/A	N/A	N/A
	3	0.0265226	172.72727	>60 min	>60 min	N/A	N/A	N/A	N/A
	5	0.0159155	47.878788	>60 min	>60 min	N/A	N/A	N/A	N/A
250	2	0.0397887	58.787879	0.0396074	58.825	-0.0001813	0.037121	-0.455657	0.063144
	3	0.0265226	358.18182	0.0264458	358.687	-0.0000768	0.50518	-0.2895644	0.1410401
	5	0.0159155	236.9697	>60 min	>60 min	N/A	N/A	N/A	N/A
50	2	0.0397887	155.75758	0.0397893	156.212	0.0000006	0.45442	0.001508	0.2917482
	3	0.0265226	143.63636	0.0264342	144.218	-0.0000884	0.58164	-0.3333007	0.4049393
	5	0.0159155	119.39394	0.0157441	119.928	-0.0001714	0.53406	-1.0769376	0.4473091

Table 9. Comparison of Green's Function with LSVOCN for Test Case 2 (Vary Horizontal Range) - $n^2(y)$ with Positive Gradient.

As a final note on the second Green's function test case, as can be observed from Tables 8 and 9, the delta magnitudes all agree out to three significant digits, and in some cases better. This fact was consistent with the magnitude differences as calculated in the first Green's function test case. Also, for small velocity potential phases, small phase errors result in large percentage differences, as expected.

3. Green's Function Test Case Three - Vary the Receiver Depth

The third Green's function test case involved varying the receiver depth above and below the source depth, while maintaining the source and surface sound-speeds fixed at 1515/1485 m/s and 1500 m/s, respectively. As was stated before, the modeled ocean medium is not homogeneous; however, for the previous two Green's function tests, the receiver depth was maintained at the source depth and the source sound-speed was varied to more closely match the surface sound-speed (Test Case 1) or maintained constant (Test Case 2) which simulated a homogeneous ocean medium. For this case, the receiver was moved slightly above and below the source depth, and as a result, the Green's function results are less valid. As can be seen from Figure 9, even though the receiver is not located at the source depth, the actual change in the sound speed at the receiver is very small. Because the ocean medium acts very much like a homogeneous medium when receivers and sources are "close", the velocity potential (magnitude and phase) computed using the free-space Green's function for a homogeneous ocean medium is a valid approximation. This test case allowed us to validate the remaining part of the computer code in LSVOCN for a source and receiver at different depths, prior to comparing it with the RRA Algorithm. This test case was conducted with a source operating at 1000 Hz (excluding cases for the source operating at 250 Hz and 50 Hz since validation at one frequency was adequate). The third Green's function test case is summarized in Table 10. The test case was conducted four times:

1. For the square of the index of refraction with a negative gradient and a receiver depth of 150.5 meters and a horizontal range of 0.8660254 meters.

2. For the square of the index of refraction with a negative gradient and a receiver depth of 149.5 meters and a horizontal range of 0.8660254 meters.

3. For the square of the index of refraction with a positive gradient and a receiver depth of 150.5 meters and a horizontal range of 0.8660254 meters.

4. For the square of the index of refraction with a positive gradient and a receiver depth of 149.5 meters and a horizontal range of 0.8660254 meters.

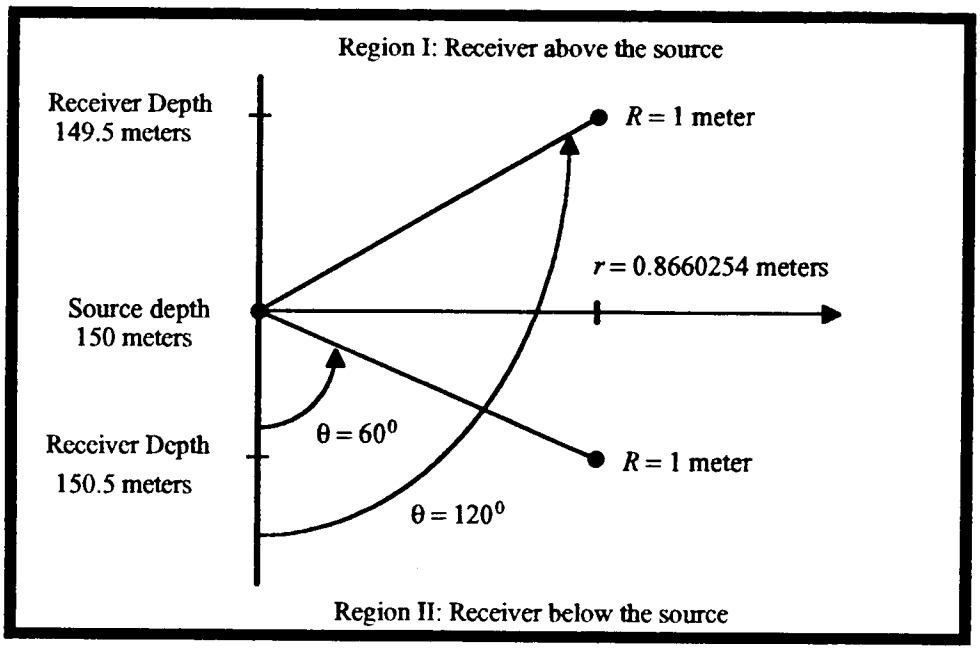

Figure 9. Geometry for Green's Function Test Case 3 (Vary Receiver Depth).

The surface sound-speed is maintained at 1500 m/s. The source sound-speed is maintained at 1515 m/s when the square of the index of refraction has a negative gradient, and 1485 m/s when the square of the index of refraction has a positive gradient. Calculations are based on Eq.(3.4) and Eq.(3.5) where R and c are treated as variables. As can be observed from Table 10, the change in the sound speed at the location of the receiver is very small, making our assumptions for this test case reasonable. Analysis of the data presented in Table 10 show that LSVOCN calculated values for the velocity potential (magnitude and phase) are approximately equal to those predicted by the Green's function - our third validation. The Delta's and percentage differences were calculated in the same manner as discussed before.

SURFACE SOUND-SPEED = 1500 M/S r = 0.8660254 METERS, FREQ = 1000 Hz										
Source Sound Speed m/s	Receiver Sound Speed m/s	Receiver Depth meters	Green's Func Magnitude m^2/s	Green's Func Phase deg.	LSVOCN Mag m^2/s	LSVOCN Phase deg.	Delta Mag m^2/s	Delta Phase deg.	% Diff Mag	% Diff Phase
1515	1514.9492501	149.5	0.0795775	302.3683	0.0795773	302.37	-0.0000002	0.0017	-0.0002513	0.0005622
1515	1515.0507551	150.5	0.0795775	302.3842	0.079575	302.381	-0.0000025	-0.0032	-0.0031416	-0.0010583
1485	1485.0492549	149.5	0.0795775	297.5838	0.079575	297.58	-0.0000025	-0.0038	-0.0031416	-0.001277
1485	1484.95075	150.5	0.0795775	297.5677	0.079577	297.569	-0.0000005	0.0013	-0.0006283	0.0004369

Table 10. Comparison of Green's Function with LSVOCN for Test Case 3 (Vary the Receiver Depth) - $n^2(y)$ with Negative and Positive Gradients.

C. COMPARISON OF LSVOCN WITH THE RECURSIVE RAY ACOUSTICS ALGORITHM

1. Test Preparation

The RRA Algorithm calculates the magnitude in Pascals and phase in degrees of the acoustic pressure along a ray path. The source is modeled as a time-harmonic, omnidirectional point source, with its strength represented by a source level (SL) value in decibels relative to one micro-pascal (rms). The "Airy function solution" is in terms of velocity potentials and is based on a time-harmonic, omnidirectional point source modeled by a unit amplitude impulse function. Thus, before the magnitudes and phases from the RRA Algorithm and LSVOCN (the "Airy function solution") could be compared, the velocity potential expressions were transformed into acoustic pressure expressions using the following equation for time-harmonic fields [Ref. 2, Chapter 2]:

$$p_f(r,y) = -j2\pi f \rho_0 \varphi_f(r,y) \tag{3.16}$$

where f is the frequency of the source in Hz, and ρ_0 is the ambient or equilibrium density of the fluid medium in kg/m^3.

In addition, the magnitudes from LSVOCN had to be made equivalent to the magnitudes computed by the RRA Algorithm by relating the source level in decibels to the amplitude of the impulse function used to model the omnidirectional point source in LSVOCN. This was accomplished by deriving a magnitude scale factor that relates a

source level in decibels to the source strength of a spherical sound source operating in the monopole mode of vibration as the radius of the sphere approaches zero [see Eq.(3.3)]. Thus, substituting Eq.(3.3) into Eq.(3.16) yields

$$p_f(R,\theta,\psi) = +jf\rho_0 S_0 \frac{\exp(-jkR)}{2R}, \; R > 0. \tag{3.17}$$

The magnitude of Eq.(3.17) is given by

$$|p_f(R,\theta,\psi)| = \frac{f\rho_0}{2R} S_0, \; R > 0. \tag{3.18}$$

Thus, the peak acoustic pressure, P_0, at R equal to one meter is

$$P_0 = |p_f(R,\theta,\psi)|_{R=1} = \frac{f\rho_0}{2} S_0 . \tag{3.19}$$

Therefore, the source strength, S_o, in m^3/s, is given by

$$S_0 = \frac{2P_0}{f\rho_0}. \tag{3.20}$$

The peak acoustic pressure, P_0, in Pascals [Ref. 2, Chapter 1] due to a given source level in decibels is given by:

$$P_0 = \sqrt{2}\, P_{ref} 10^{\left(\frac{SL}{20}\right)} \tag{3.21}$$

where P_{ref} is the reference pressure equal to one micro-pascal (rms), and SL is the source level of the source in decibels relative to P_{ref}. Since the source level used by the RRA Algorithm is a known constant (180.0 dB), the peak acoustic pressure can be calculated using Eq.(3.21). This result can then be substituted into Eq.(3.20) allowing the source

strength to be computed. The resulting source strength value, S_0, is the magnitude scale factor that was used to multiply the output from LSVOCN.

In summary, the conversion process to make the LSVOCN magnitude and phase equivalent to that computed by the RRA Algorithm is as follows [multiply the right-hand side of Eq.(3.16) by Eq.(3.20)]:

$$p_f(r,y) = -j2\pi f \rho_0 \frac{2P_0}{f\rho_0}\varphi_f(r,y) = -j4\pi P_0 \varphi_f(r,y), \tag{3.22}$$

where P_0 is given by Eq.(3.21). Equation (3.22) was added as FORTRAN computer code to LSVOCN so that the conversion process would be taken care of automatically.

2. Comparison of the RRA Algorithm with LSVOCN when $n^2(y)$ has a Negative Gradient

The RRA Algorithm was used to simulate various ray paths propagated through the ocean medium when the square of the index of refraction was a linear function of depth with a negative gradient, corresponding to a positive gradient sound-speed profile. Two ray paths identified by the initial launch angle, β_o, were selected for each of the test frequencies, 1000 Hz, 250 Hz, and 50 Hz. The sound-speed profile and the ray propagation path for each ray is illustrated in Figure 10. Launch angles were selected so that the ray paths did not interact with the ocean surface or bottom, thus ensuring that the magnitude and phase calculated by the RRA Algorithm were for a free-space propagation problem. Test points along each ray path were selected. The depth (receiver depth) and the horizontal range (HRNG) corresponding to these points were recorded and used as inputs to LSVOCN. The comparison between the RRA Algorithm and LSVOCN magnitude and phase values are summarized in Tables 11 through 13, where the asterisk "*" means that the entire row corresponds to data at the location of a turning point. The calculated values in Tables 11 through 13 were obtained as follows:

1. Delta magnitude = RRA Magnitude - LSVOCN Magnitude

2. Delta phase = RRA Phase - LSVOCN Phase

3. Initial phase offset = Delta phase of the first point for each ray

4. Adj RRA Phase = (RRA Phase - Initial phase offset)
   a) Add 360° if Adj RRA Phase angle is negative
   b) Subtract 360° if Adj RRA Phase angle is greater than 360°
   c) Do not add or subtract if Adj RRA Phase angle is positive and less than 360°

$$5.\ \%\ \text{Difference Magnitude} = \frac{\text{RRA Magnitude - LSVOCN Magnitude}}{\text{LSVOCN Magnitude}} \times 100\%$$

$$6.\ \%\ \text{Difference Phase} = \frac{\text{Adj RRA Phase - LSVOCN Phase}}{\text{LSVOCN Phase}} \times 100\%$$

Analysis of the data if Tables 11 through 13 indicate that the magnitudes and phases calculated by the RRA Algorithm match reasonably well with the magnitudes and phases calculated by LSVOCN. Note that there is an initial phase difference that exists between the RRA Algorithm and LSVOCN. The RRA Algorithm begins with zero phase and calculates the phase thereafter based on travel time as a ray propagates. In order to correct for this initial phase difference, each RRA phase angle after the first data point on each ray is adjusted by an amount equal to the delta phase of the first data point. After the RRA phase has been adjusted, a valid comparison between the RRA phase and LSVOCN phase can be performed. It can further be observed that the percentage phase error tends to increase as the ray propagates. This seems reasonable since small errors made in calculating travel time and, hence, phase in the beginning accumulate as the ray propagates further from the source. These phase errors could possibly be reduced by selecting a smaller arc length step size used by the RRA Algorithm.

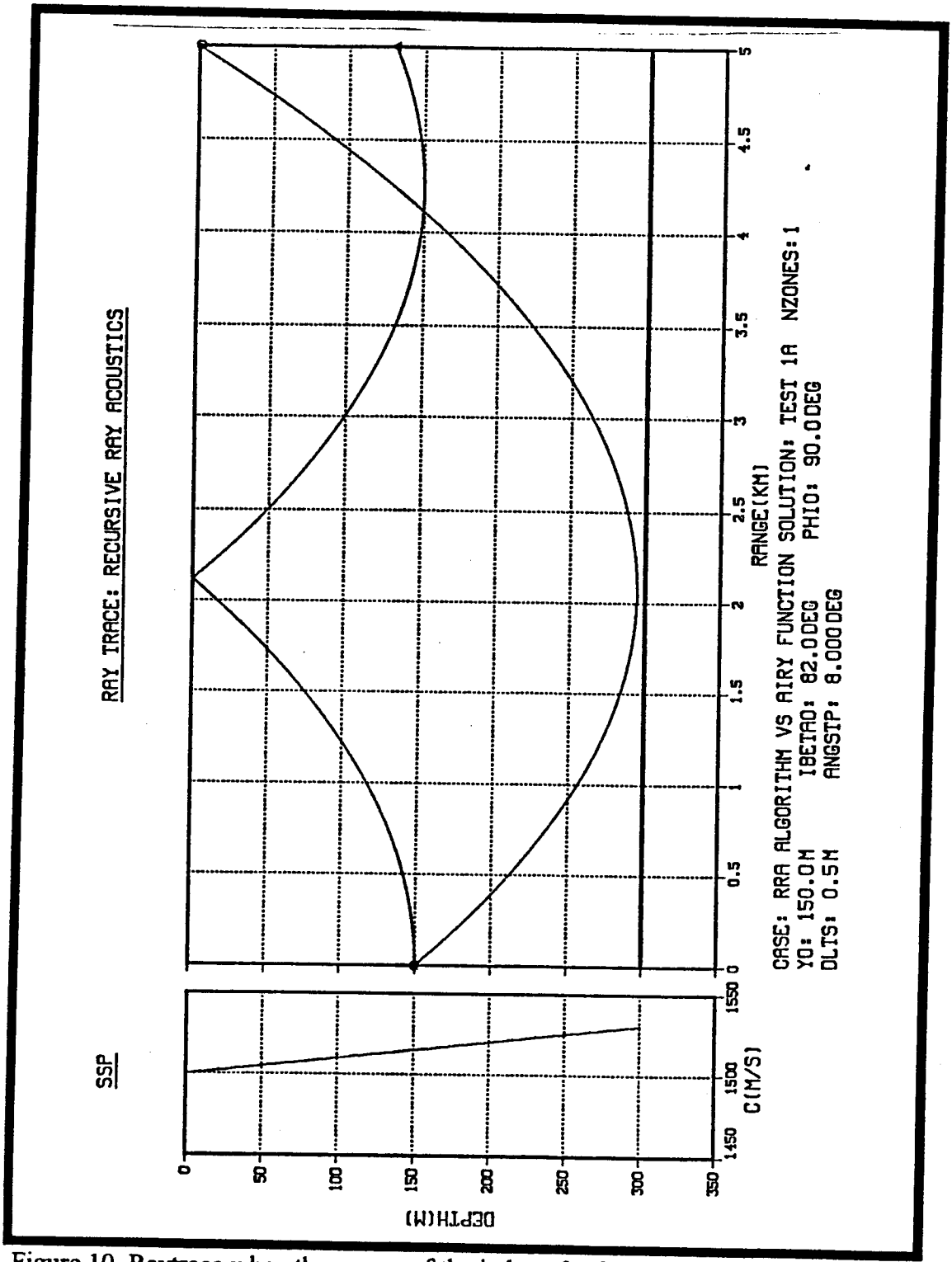

Figure 10. Raytrace when the square of the index of refraction is a linear function of depth with a negative gradient for two separate ray paths with $\beta_0 = 82^0$ and 90^0.

SURFACE SOUND-SPEED = 1500 m/s, SOURCE-SOUND SPEED = 1515 m/s SOURCE DEPTH = 150 m, $n^2(y)$ WITH NEGATIVE GRADIENT FREQUENCY = 1000 HZ, "*" TURNING POINT DATA										
Receiver Depth meters	Receiver HRNG meters	RRA Mag Pascals	RRA Phase Degree	LSVOCN Mag Pascals	LSVOCN Phase Degrees	DELTA Mag Pascals	DELTA Phase Degrees	Adj RRA Phase Degrees	% DIFF Mag	% DIFF Phase
β_o=82°										
150.139	0.99	1414.21	122.377	1414.06	212.411	0.15	-90.034	N/A	0.01061	N/A
211.757	500.178	2.80646	17.022	2.79558	107.978	0.01088	-90.956	107.056	0.38919	-0.85388
256.408	1000.164	1.40685	215.202	1.39683	303.34	0.01002	-88.138	305.236	0.71734	0.62504
283.987	1500.38	0.94006	219.763	0.9673	307.452	-0.02725	-87.689	309.797	-2.81609	0.76272
* 294.58	2056.996	0.68751	218.93	0.6809	304.917	0.00661	-85.987	308.964	0.97077	1.32725
223.48	3499.913	0.40689	145.679	0.43452	241.2	-0.02762	-95.521	235.713	-6.35874	-2.27488
90.742	4499.953	0.31804	348.299	0.2707	75.886	0.04733	272.413	78.333	17.48799	3.22457
1	4988.762	0.28757	238.727	0.30947	337.044	-0.0219	-98.317	326.865	-7.07661	-3.02008
β_o=90°										
150	1	1414.21	122.376	1410.77	212.154	3.44	-89.778	N/A	0.24384	N/A
141.636	499.907	2.82896	325.936	2.83278	56.813	-0.00382	269.123	55.714	-0.13485	-1.93442
116.533	999.753	1.41456	39.786	1.44011	131.49	-0.02555	-91.704	129.564	-1.77417	-1.46475
74.652	1499.98	0.94282	209.696	0.96954	302.063	-0.02672	-92.367	299.474	-2.75595	-0.85711
16.029	2000.033	0.7071	341.127	0.66581	69.119	0.04129	272.008	70.905	6.20147	2.58395

Table 11. Comparison of RRA Algorithm with LSVOCN Magnitude and Phase Values for different Receiver Depth and Horizontal Range Points Located on Two Separate Sound Rays, Identified by β_o.

SURFACE SOUND-SPEED = 1500 m/s, SOURCE SOUND-SPEED = 1515 m/s SOURCE DEPTH = 150 m, $n^2(y)$ WITH NEGATIVE GRADIENT FREQUENCY = 250 HZ, "*" TURNING POINT DATA										
Receiver Depth meters	Receiver HRNG meters	RRA Mag Pascals	RRA Phase Degree	LSVOCN Mag Pascals	LSVOCN Phase Degrees	DELTA Mag Pascals	DELTA Phase Degrees	Adj RRA Phase Degrees	% DIFF Mag	% DIFF Phase
β_o=82°										
150.139	0.99	1414.21	300.594	1415.07	30.646	-0.86	269.948	N/A	-0.06077	N/A
211.757	500.178	2.80646	4.255	2.80952	93.273	-0.00306	-89.018	94.307	-0.10892	1.10857
256.408	1000.164	1.40685	233.8	1.37561	325.296	0.03124	-91.496	323.852	2.27099	-0.4439
283.987	1500.38	0.94006	234.941	0.90205	326.776	0.03801	-91.835	324.993	4.21374	-0.54563
* 294.58	2056.996	0.68751	234.732	0.65279	321.869	0.03472	-87.137	324.784	5.31871	0.90565
223.48	3499.913	0.40689	36.42	0.41643	133.076	-0.00954	-96.656	126.472	-2.2909	-4.96258
90.742	4499.953	0.31804	267.075	0.27485	352.622	0.04319	-85.547	357.127	15.71403	1.27757
1	4988.762	0.28757	59.682	0.2389	151.482	0.04867	-91.8	149.734	20.37254	-1.15393
β_o=90°										
150	1	1414.21	300.594	1415.54	30.689	-1.33	269.905	N/A	-0.09396	N/A
141.636	499.907	2.82896	171.484	2.82851	260.489	0.00045	-89.005	261.579	0.01591	0.41844
116.533	999.753	1.41456	279.946	1.42205	11.855	-0.00749	268.091	10.041	-0.5267	-15.30156
74.652	1499.98	0.94282	232.424	0.98967	322.027	-0.04685	-89.603	322.519	-4.7339	0.15278
16.029	2000.033	0.7071	355.282	0.7486	87.039	-0.0415	268.243	85.377	-5.54368	-1.90949

Table 12. Comparison of RRA Algorithm with LSVOCN Magnitude and Phase Values for different Receiver Depth and Horizontal Range Points Located on Two Separate Sound Rays, Identified by β_o.

SURFACE SOUND-SPEED = 1500 m/s, SOURCE SOUND-SPEED = 1515 m/s SOURCE DEPTH = 150 m, $n^2(y)$ WITH NEGATIVE GRADIENT FREQUENCY = 50 HZ, "*" TURNING POINT DATA										
Receiver Depth meters	Receiver HRNG meters	RRA Mag Pascals	RRA Phase Degree	LSVOCN Mag Pascals	LSVOCN Phase Degrees	DELTA Mag Pascals	DELTA Phase Degrees	Adj RRA Phase Degrees	% DIFF Mag	% DIFF Phase
β_o=82°										
150.139	0.99	1414.21	348.119	1396.42	77.964	17.79	270.155	N/A	1.27397	N/A
211.757	500.178	2.80646	144.851	2.7779	235.583	0.02856	-90.732	234.696	1.02811	-0.37651
256.408	1000.164	1.40685	334.76	1.44067	63.371	-0.03382	271.389	64.605	-2.34752	1.94726
283.987	1500.38	0.94006	190.988	0.89268	281.376	0.04738	-90.388	280.833	5.30761	-0.19298
* 294.58	2056.996	0.68751	118.946	0.7305	207.172	-0.04299	-88.226	208.791	-5.88501	0.78148
223.48	3499.913	0.40689	7.284	0..361466	99.872	0.04542	-92.588	97.129	12.66604	-2.74652
90.742	4499.953	0.31804	269.415	0.36089	355.423	-0.04285	-86.008	359.26	-11.87342	1.07956
1	4988.762	0.28757	83.936	0.32794	168.751	-0.04037	-84.815	173.781	-12.31018	2.98072
β_o=90°										
150	1	1414.21	348.119	1425.34	78.211	-11.13	269.908	N/A	-0.78087	N/A
141.636	499.907	2.82896	178.297	2.8749	267.929	-0.04594	-89.632	268.389	-1.59797	0.17169
116.533	999.753	1.41456	343.989	1.4166	75.872	-0.00204	268.117	74.081	-0.14401	-2.36055
74.652	1499.98	0.94282	118.485	0.95694	205.742	-0.01412	-87.257	208.577	-1.47554	1.37794
16.029	2000.033	0.7071	215.056	0.67256	302.346	0.03454	-87.29	305.148	5.1356	0.92675

Table 13. Comparison of RRA Algorithm with LSVOCN Magnitude and Phase Values for different Receiver Depth and Horizontal Range Points Located on Two Separate Sound Rays, Identified by β_o.

3. Comparison of the RRA Algorithm with LSVOCN when $n^2(y)$ has a Positive Gradient

The RRA Algorithm was used to simulate various ray paths propagated through the ocean medium when the square of the index of refraction was a linear function of depth with a positive gradient, corresponding to a negative gradient sound-speed profile. Two ray paths identified by the initial launch angle, β_o, were selected for each of the test frequencies, 1000 Hz, 250 Hz, and 50 Hz. The sound-speed profile and the ray propagation path for each ray is illustrated in Figure 11. Launch angles were selected so that the ray paths did not interact with the ocean surface or bottom, thus ensuring that the magnitude and phase calculated by the RRA Algorithm were for a free-space propagation problem. Test points along each ray path were selected. The depth (receiver depth) and the horizontal range (HRNG) corresponding to these points were recorded and used as inputs to LSVOCN. The comparison between the RRA Algorithm and LSVOCN magnitude and phase values are summarized in Tables 14 through 16, where the asterisk "*" means that the entire row corresponds to data at the location of a turning point. The

calculated values in Tables 14 through 16 were obtained in the same manner as was done for Tables 11 through 13. Analysis of the data in Tables 14 through 16 indicate that the magnitudes and phases calculated by the RRA Algorithm match reasonably well with the magnitudes and phases calculated by LSVOCN. Note that there is an initial phase difference that exists between the RRA Algorithm and LSVOCN. The RRA Algorithm begins with zero phase and calculates the phase thereafter based on travel time as a ray propagates. In order to correct for this initial phase difference, each RRA phase angle after the first data point on each ray is adjusted by an amount equal to the first delta phase of the first data point. After the RRA phase has been adjusted, a valid comparison between the RRA phase and LSVOCN phase can be performed. It can further be observed that the percentage phase error tends to increase as the ray propagates. This seems reasonable since small errors in the beginning accumulate as the ray propagates further from the source. These phase errors could possibly be reduced by selecting a smaller arc length step size used by the RRA Algorithm. Also, for small acoustic pressure phases, small errors result in large percentage differences, as expected.

SURFACE SOUND-SPEED = 1500 m/s, SOURCE SOUND-SPEED = 1485 m/s
SOURCE DEPTH = 150 m, $n^2(y)$ WITH POSITIVE GRADIENT
FREQUENCY = 1000 HZ, "*" TURNING POINT DATA

Receiver Depth meters	Receiver HRNG meters	RRA Mag Pascals	RRA Phase Degree	LSVOCN Mag Pascals	LSVOCN Phase Degrees	DELTA Mag Pascals	DELTA Phase Degrees	RRA Adj Phase Degrees	% DIFF Mag	% DIFF Phase
β_o=98°										
149.861	0.99	1414.21	117.577	1414.14	207.61	0.07	-90.033	N/A	0.00495	N/A
88.159	500.168	2.80645	120.409	2.82886	209.598	-0.02241	-89.189	210.442	-0.79219	0.40268
43.255	1000.132	1.40682	77.211	1.36943	166.044	0.03739	-88.833	167.244	2.73033	0.7227
15.25	1500.325	0.94002	210.833	0.97634	299.001	-0.03631	-88.168	300.866	-3.72002	0.62374
* 3.967	2077.678	0.68067	138.344	0.64677	231.267	0.03389	-92.923	228.377	5.24143	-1.24964
72.257	3498.868	0.40695	270.66	0.38583	6.948	0.02111	263.712	0.693	5.47391	-90.02591
202.264	4499.27	0.31802	42.263	0.36148	135.816	-0.04346	-93.553	132.296	-12.0228	-2.59174
290.462	4988.36	0.28753	120.254	0.23971	208.418	0.04781	-88.164	209.087	19.94911	0.32099
β_o=90°										
150	1	1414.21	117.576	1399.25	207.709	14.96	-90.133	N/A	1.06914	N/A
158.268	499.534	2.83107	176.655	2.78723	266.248	0.04384	-89.593	266.788	1.57289	0.20282
183.11	999.394	1.41507	8.009	1.45581	97.086	-0.04074	-89.077	98.142	-2.79844	1.0877
224.566	1499.657	0.94303	288.292	0.95899	20.833	-0.01597	267.459	18.425	-1.66425	-11.55858
282.604	1999.778	0.70719	162.897	0.70929	249.048	-0.00211	-86.151	253.03	-0.29607	1.59889

Table 14. Comparison of RRA Algorithm with LSVOCN Magnitude and Phase Values for different Receiver Depth and Horizontal Range Points Located on Two Separate Sound Rays, Identified by β_o.

SURFACE SOUND-SPEED = 1500 m/s, SOURCE SOUND-SPEED = 1485 m/s SOURCE DEPTH = 150 m, $n^2(y)$ WITH POSITIVE GRADIENT FREQUENCY = 250 HZ, "*" TURNING POINT DATA										
Receiver Depth meters	Receiver HRNG meters	RRA Mag Pascals	RRA Phase Degree	LSVOCN Mag Pascals	LSVOCN Phase Degrees	DELTA Mag Pascals	DELTA Phase Degrees	RRA Adj Phase Degrees	% DIFF Mag	% DIFF Phase
β_o=98°										
149.861	0.99	1414.21	299.394	1415.07	29.447	–0.86	269.947	N/A	–0.06077	N/A
88.159	500.168	2.80645	120.102	2.77775	209.334	0.0287	–89.232	210.155	1.03321	0.3922
43.255	1000.132	1.40682	109.303	1.44734	200.284	–0.04052	–90.981	199.356	–2.79962	–0.46334
15.25	1500.325	0.94002	232.708	0.98028	321.198	–0.04026	–88.49	322.761	–4.10699	0.48662
* 3.967	2077.678	0.68067	124.586	0.67268	218.573	0.00799	–93.987	214.639	1.18779	–1.79986
72.257	3498.868	0.40695	247.665	0.4037	344.465	0.00325	–96.8	337.718	0.80505	–1.95869
202.264	4499.27	0.31802	10.566	0.30859	91.865	0.00943	–81.299	100.619	3.05583	9.5292
290.462	4988.36	0.28753	300.064	0.33218	33.548	–0.04464	266.516	30.117	–13.44151	–10.22714
β_o=90°										
150	1	1414.21	299.394	1406.07	29.774	8.14	269.62	N/A	0.57892	N/A
158.268	499.534	2.83107	314.164	2.80951	44.984	0.02156	269.18	44.544	0.76739	–0.97813
183.11	999.394	1.41507	182.002	1.37475	272.98	0.04032	–90.978	272.382	2.9329	–0.21906
224.566	1499.657	0.94303	252.073	0.94032	339.194	0.00271	–87.121	342.453	0.2882	0.96081
282.604	1999.778	0.70719	130.724	0.67483	223.51	0.03236	–92.786	221.104	4.79528	–1.07646

Table 15. Comparison of RRA Algorithm with LSVOCN Magnitude and Phase Values for different Receiver Depth and Horizontal Range Points Located on Two Separate Sound Rays, Identified by β_o.

SURFACE SOUND-SPEED = 1500 m/s, SOURCE SOUND-SPEED = 1485 m/s SOURCE DEPTH = 150 m, $n^2(y)$ WITH POSITIVE GRADIENT FREQUENCY = 50 HZ, "*" TURNING POINT DATA										
Receiver Depth meters	Receiver HRNG meters	RRA Mag Pascals	RRA Phase Degree	LSVOCN Mag Pascals	LSVOCN Phase Degrees	DELTA Mag Pascals	DELTA Phase Degrees	RRA Adj Phase Degrees	% DIFF Mag	% DIFF Phase
β_o=98°										
149.861	0.99	1414.21	347.879	1395.57	77.713	18.64	270.166	N/A	1.33565	N/A
88.159	500.168	2.80645	24.02	2.8002	112.986	0.00625	-88.966	113.854	0.2232	0.76824
43.255	1000.132	1.40682	93.861	1.37231	182.489	0.03451	-88.628	183.695	2.51474	0.66086
15.25	1500.325	0.94002	190.542	0.89886	279.047	0.04116	-88.505	280.376	4.57913	0.47626
* 3.967	2077.678	0.68067	96.917	0.72557	188.197	-0.0449	-91.28	186.751	-6.18824	-0.76834
72.257	3498.868	0.40695	265.533	0.43785	350.513	-0.0309	-84.98	355.367	-7.05721	1.38483
202.264	4499.27	0.31802	290.113	0.36357	17.357	-0.04555	272.756	19.947	-12.52854	14.92193
290.462	4988.36	0.28753	348.013	0.3022	86.994	-0.01467	261.019	77.847	-4.8544	-10.51452
β_o=90°										
150	1	1414.21	347.879	1417.16	78.123	-2.95	269.756	N/A	-0.20816	N/A
158.268	499.534	2.83107	62.833	2.82662	153.724	0.00445	-90.891	153.077	0.15743	-0.42088
183.11	999.394	1.41507	108.4	1.45024	197.13	-0.03517	-88.73	198.644	-2.42512	0.76802
224.566	1499.657	0.94303	122.415	0.94316	209.544	-0.00013	-87.129	212.659	-0.01378	1.48656
282.604	1999.778	0.70719	98.145	0.74101	185.56	-0.03382	-87.415	188.389	-4.56404	1.52457

Table 16. Comparison of RRA Algorithm with LSVOCN Magnitude and Phase Values for different Receiver Depth and Horizontal Range Points Located on Two Separate Sound Rays, Identified by β_o.

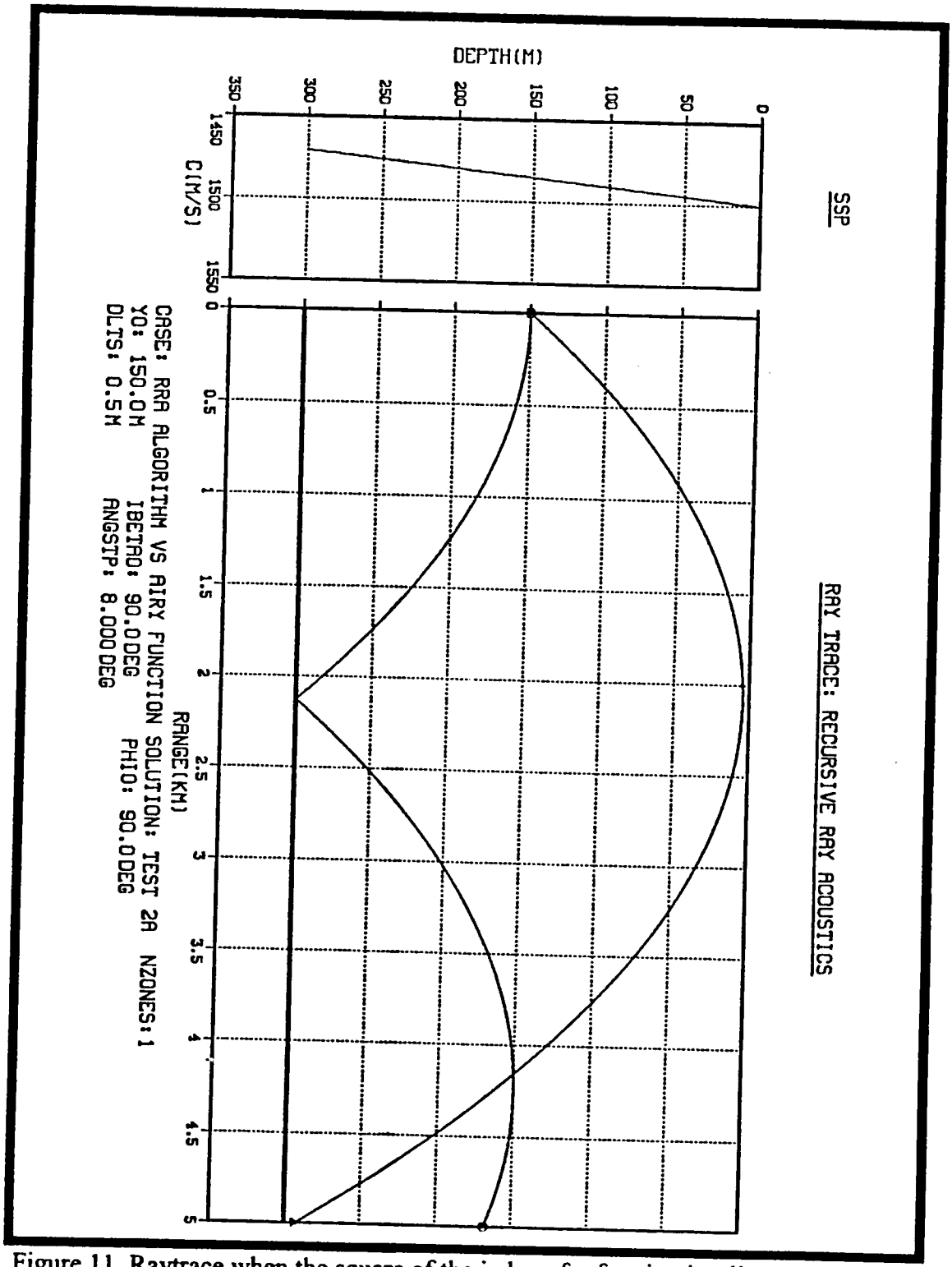

Figure 11. Raytrace when the square of the index of refraction is a linear function of depth with a positive gradient for two separate ray paths with $\beta_o = 90^o$ and $\beta_o = 98^o$.

IV. SUMMARY AND RECOMMENDATIONS

This thesis had two primary goals. First, derive and document the solution to the three-dimensional inhomogeneous Helmholtz equation for a free-space propagation problem when the square of the index of refraction of the ocean medium is a linear function of depth, and the source is an omindirectional point source. Given this type of index of refraction, the solution to the inhomogeneous Helmholtz equation has an exact solution in terms of Airy functions. This exact solution, in terms of Airy functions, was then incorporated into the computer program Linear Space-Variant Ocean (LSVOCN) as an additional ocean medium transfer function. The second goal was to further test the Recursive Ray Acoustics (RRA) Algorithm by comparing the magnitudes and phases of the acoustic sound pressure calculated, at various points, along a ray path generated by the RRA Algorithm with corresponding magnitudes and phases calculated by LSVOCN along the same ray path.

In Chapter II, the solution to the aforementioned Helmholtz equation was carefully derived and documented. This documentation served to record in detail the steps that led to the final Airy function solution.

The next step in the solution process was to convert the theoretical Airy function solution to the FORTRAN computer code that was used by LSVOCN. The main problems in the conversion process were the many numerical errors that developed. There were two main numerical errors encountered, overflow and underflow errors. Overflow errors resulted from the evaluation of the Bairy function with large positive argument values. The Airy function did not have this problem since it is well behaved for both negative and positive argument values. A graphical representation of both the Airy and Bairy functions is shown in Figures 7 and 8, respectively. Overflow errors result in the termination of the computer code before it has finished a calculation. Thus no answer is ever obtained - a serious problem. To prevent overflow errors, we used the exponentially scaled Airy and Bairy functions, also shown in Figures 7 and 8. These two functions allowed a significant advance towards a working FORTRAN computer code that would solve the "Airy function solution" as given by Eq.(2.75) through Eq.(2.78).

Using the exponentially scaled functions allowed for very large positive values of $\zeta(y)$, the argument of the Airy and Bairy functions, to be used. These large positive values of $\zeta(y)$ were the result of propagating waves becoming evanescent waves. For the solution to be accurate, it is very important to account for these evanescent waves. The exponentially scaled functions did not prevent underflow errors. These types of errors do introduce some numerical inaccuracies, but do not result in computer program termination.

The last numerical problem to solve was to establish an upper limit of integration for Eq.(2.3). Using the computer, it is impossible to literally integrate to infinity. To achieve numerical accuracy, the upper limit of integration had to be large enough to account for most of the significant evanescent waves. Thus, a method to automatically compute this upper limit of integration, regardless of the source frequency selected, was developed.

Before comparing the RRA Algorithm with LSVOCN, we developed test cases to validate the Airy function solution and FORTRAN computer code used by LSVOCN. This validation was carried out by comparing the magnitude and phase of the velocity potential equal to the free-space Green's function of a homogeneous ocean medium with the magnitude and phase of the velocity potential computed by LSVOCN. The free-space Green's function was chosen because we could make the modeled ocean medium used by LSVOCN "simulate" a homogeneous medium without actually being made homogeneous. Therefore, the Green's function provided a simple theoretical solution that we could compare the calculated solution of LSVOCN with. All three Green's function test cases discussed in detail in Chapter III gave very good results. Now we were finally ready to test calculated values from the Recursive Ray Acoustics (RRA) Algorithm with those predicted by LSVOCN.

The RRA Algorithm versus LSVOCN comparison tests were conducted first, when the square of the index of refraction had a negative gradient and second, when the square of the index of refraction had a positive gradient. The test results indicated that the magnitudes from the RRA Algorithm and LSVOCN were in close agreement. In

order to be able to compare the RRA Algorithm with LSVOCN, a magnitude scale factor was derived that related the source level in decibels used by the RRA Algorithm to the amplitude of the impulse function used to model the omnidirectional point source in LSVOCN. The magnitudes of LSVOCN were extremely close to the values predicted by the RRA Algorithm.

The phase comparisons between the RRA Algorithm and LSVOCN were also quite good. The initial phase offset between LSVOCN and the RRA Algorithm was determined by calculating the phase differences, one meter from the source, between the RRA Algorithm and LSVOCN, i.e., the phase difference between the RRA Algorithm and LSVOCN of the first data point of each ray path. Once this difference was determined, it was subtracted from the other phase values, less the first data point, calculated by the RRA Algorithm along the same ray path. It was observed that the percentage phase error tended to grow as the receiver was moved further from the source. This trend makes intuitive sense because it suggests that small phase errors in the beginning are propagated and accumulated as the ray travels further from the source. It was also observed that several data points resulted in large percentage differences for the phase. These large percentage differences, resulting from the variance between small phases could possibly be reduced by making the integration step size a function of the wave number rather than a fixed quantity.

Because ray acoustics is an approximate solution of the wave equation, characterized as a "high frequency" approximation, we expected to see better and better agreement between the RRA Algorithm and LSVOCN as the source frequency increased from 50 Hertz to 1000 Hertz. The data in Tables 11 through 16 did not indicate such a trend for all cases. In fact, some percentage errors in magnitude and phase are larger for the 1000 Hertz case than the 50 Hertz case. The expected results could possibly be observed if the integration step size were made a function of the wave number, as discussed earlier. The results from all six test cases comparing the RRA Algorithm with LSVOCN indicate that the RRA Algorithm was, in general, accurate regardless of the frequency selected.

As a final note, the CPU time required by the RRA Algorithm to compute all of the magnitudes and phases for thousands of points along each ray path was typically on the order of 30 seconds. Table 17 gives the approximate CPU times for each LSVOCN data point calculated. Examination of Table 17 reveals that the RRA Algorithm is a much more efficient method to calculate the acoustic pressure compared to the Airy function wave solution. The wave solution not only takes considerably more time, but is also more susceptible to numerical inaccuracies.

CPU TIMES PER DATA POINT CALCULATED BY LSVOCN				
	$\beta_0 = 90^0$	$\beta_0 = 82^0$	$\beta_0 = 90^0$	$\beta_0 = 98^0$
	Square of the index of refraction with Negative gradient		Square of the index of refraction with Positive gradient	
FREQ = 1000 HZ	receiver @ 1 meter ~59 min other receiver points ~6 min	receiver @ 1 meter ~50 min other receiver points ~6 min	receiver @ 1 meter ~54 min other receiver points ~6 min	receiver @ 1 meter ~22.5 min other receiver points ~6 min
FREQ = 250 HZ	receiver @ 1 meter ~ 16 min other receiver point ~5 min	receiver @ 1 meter ~ 22 min other receiver point ~5 min	receiver @ 1 meter ~ 16 min other receiver point ~5.5 min	receiver @ 1 meter ~ 23 min other receiver point ~5.3 min
FREQ = 50 HZ	receiver @ 1 meter ~8 min other receiver point ~5 min	receiver @ 1 meter ~25 min other receiver point ~5 min	receiver @ 1 meter ~8.2 min other receiver point ~4 min	receiver @ 1 meter ~26 min other receiver point ~5 min

Table 17. CPU Times Per Data Point Calculated by LSVOCN.

Recommendations for further research include:

1. To achieve more accurate calculated acoustic pressure values from the RRA Algorithm (magnitude and phase) a smaller arc length step size, used by the RRA Algorithm, should be selected. Using a smaller arc length step size may decrease small phase errors that are propagated and accumulated as the ray travels further from the source.

2. Propagate sound rays, using the RRA Algorithm, such that focal points are generated. Compare the RRA Algorithm and LSVOCN results.

3. Make the integration step size used by Eq.(2.3) a function of the wave number to determine if improved accuracy can be obtained.

APPENDIX. TABULATED VALUES FOR $n^2(y), k_y^2(y)$, and $\zeta(y)$ FOR DIFFERENT LAUNCH ANGLES AND RECEIVER DEPTHS.

	FREQUENCY = 50 HZ SOURCE DEPTH = 150 M $n^2(y)$ WITH POSITIVE GRADIENT						
	RECEIVER DEPTH						
	$y=0$ meters	$y=50$ meters	$y=100$ meters	$y=150$ meters	$y=200$ meters	$y=250$ meters	$y=300$ meters
$\beta_o = 84°$							
$n^2(y)$	0.98010	0.98673	0.99337	1.00000	1.0066	1.0133	1.0199
$k_y^2(y)$	-0.0004016	-0.0001048	0.00019213	0.00048901	0.00078589	0.0010828	0.0013796
$\zeta(y)$	1.2249	0.31946	-0.58594	-1.4913	-2.3967	-3.3021	-4.075
$\beta_o = 86°$							
$n^2(y)$	0.98010	0.98673	0.99337	1.00000	1.0066	1.0133	1.0199
$k_y^2(y)$	-0.0006729	-0.0003759	-0.0000791	0.00021778	0.00051466	0.00081154	0.0011084
$\zeta(y)$	2.0520	1.1466	0.24123	-0.66417	-1.5696	-2.4750	-3.3804
$\beta_o = 88°$							
$n^2(y)$	0.98010	0.98673	0.99337	1.00000	1.0066	1.0133	1.0199
$k_y^2(y)$	-0.0008361	-0.0005393	-0.0002424	0.00005451	0.00035139	0.00064827	0.00094515
$\zeta(y)$	2.5500	1.6446	0.73915	-0.16624	-1.0716	-1.9770	-2.8824
$\beta_o = 90°$							
$n^2(y)$	0.98010	0.98673	0.99337	1.00000	1.0066	1.0133	1.0199
$k_y^2(y)$	-0.0008906	-0.0005938	-0.0002969	0.0	0.00029688	0.00059376	0.00089064
$\zeta(y)$	2.7162	1.8108	0.90540	0.0	-0.90540	-1.8108	-2.7162
$\beta_o = 92°$							
$n^2(y)$	0.98010	0.98673	0.99337	1.00000	1.0066	1.0133	1.0199
$k_y^2(y)$	-0.0008361	-0.0005393	-0.0002424	0.00005451	0.00035139	0.00064827	0.00094515
$\zeta(y)$	2.5500	1.6446	0.73915	-0.16624	-1.0716	-1.9770	-2.8824
$\beta_o = 94°$							
$n^2(y)$	0.98010	0.98673	0.99337	1.00000	1.0066	1.0133	1.0199
$k_y^2(y)$	-0.0006729	-0.0003760	0.00019213	0.00048901	0.00078589	0.0010828	0.0011084
$\zeta(y)$	2.0520	1.1466	-0.58594	-1.4913	-2.3967	-3.3021	-3.3804
$\beta_o = 96°$							
$n^2(y)$	0.98010	0.98673	0.99337	1.00000	1.0066	1.0133	1.0199
$k_y^2(y)$	-0.0004016	-0.0001048	-0.0001028	0.00048901	0.0010847	0.0016844	0.0013796
$\zeta(y)$	1.2249	0.31946	0.031345	-1.4913	-3.3081	-5.1370	-4.2075
$\beta_o = 98°$							
$n^2(y)$	0.98010	0.98673	0.99337	1.00000	1.0066	1.0133	1.0199
$k_y^2(y)$	-0.0000238	0.00027312	0.00057000	0.00086688	0.0011638	0.0014606	0.0017575
$\zeta(y)$	0.072457	-0.83294	-1.7383	-2.6437	-3.5491	-4.4545	-5.3599

Table 18. Values of $n^2(y)$, $k_y^2(y)$, $\zeta(y)$ for different launch angles β_0 and receiver depths y.

	FREQUENCY = 250 HZ SOURCE DEPTH = 150 M $n^2(y)$ WITH POSITIVE GRADIENT						
	RECEIVER DEPTH						
	y = 0 meters	y = 50 meters	y = 100 meters	y = 150 meters	y = 200 meters	y = 250 meters	y = 300 meters
$\beta_o = 84°$							
$n^2(y)$	0.98010	0.98673	0.99337	1.00000	1.0066	1.0133	1.0199
$k_y^2(y)$	-0.010041	-0.0026187	0.0048032	0.012225	0.019647	0.027069	0.034491
$\zeta(y)$	3.5815	0.93409	-1.7133	-4.3607	-7.0081	-9.6555	-12.303
$\beta_o = 86°$							
$n^2(y)$	0.98010	0.98673	0.99337	1.00000	1.0066	1.0133	1.0199
$k_y^2(y)$	-0.016821	-0.0093994	-0.0019775	0.0054445	0.012866	0.020288	0.027710
$\zeta(y)$	6.0002	3.3528	0.70537	-1.9420	-4.5894	-7.2368	-9.8842
$\beta_o = 88°$							
$n^2(y)$	0.98010	0.98673	0.99337	1.00000	1.0066	1.0133	1.0199
$k_y^2(y)$	-0.020903	-0.013481	-0.0060592	0.0013628	0.0087847	0.016207	0.023629
$\zeta(y)$	7.4561	4.8087	2.1613	-0.48610	-3.1335	-5.7809	-8.4283
$\beta_o = 90°$							
$n^2(y)$	0.98010	0.98673	0.99337	1.00000	1.0066	1.0133	1.0199
$k_y^2(y)$	-0.022266	-0.014844	-0.0074220	0.0	0.0074220	0.014844	0.022266
$\zeta(y)$	7.9422	5.2948	2.6474	0.0	-2.6474	-5.2948	-7.9422
$\beta_o = 92°$							
$n^2(y)$	0.98010	0.98673	0.99337	1.00000	1.0066	1.0133	1.0199
$k_y^2(y)$	-0.020903	-0.013481	-0.0060592	0.0013628	0.0087847	0.016207	0.023629
$\zeta(y)$	7.4561	4.8087	2.1613	-0.48610	-3.1335	-5.7809	-8.4283
$\beta_o = 94°$							
$n^2(y)$	0.98010	0.98673	0.99337	1.00000	1.0066	1.0133	1.0199
$k_y^2(y)$	-0.016821	-0.0093994	-0.0019775	0.0054445	0.012866	0.020288	0.027710
$\zeta(y)$	6.0002	3.3528	0.70537	-1.9420	-4.5894	-7.2368	-9.8842
$\beta_o = 96°$							
$n^2(y)$	0.98010	0.98673	0.99337	1.00000	1.0066	1.0133	1.0199
$k_y^2(y)$	-0.010041	-0.0026187	0.0048032	0.012225	0.019647	0.027069	0.034491
$\zeta(y)$	3.5815	0.93409	-1.7133	-4.3607	-7.0081	-9.6555	-12.303
$\beta_o = 98°$							
$n^2(y)$	0.98010	0.98673	0.99337	1.00000	1.0066	1.0133	1.0199
$k_y^2(y)$	-0.0005940	0.0068280	0.014250	0.021672	0.029094	0.036516	0.043938
$\zeta(y)$	0.21186	-2.4355	-5.0829	-7.7303	-10.378	-13.025	-15.673

Table 19. Values of $n^2(y)$, $k_y^2(y)$, $\zeta(y)$ for different launch angles β_0 and receiver depths y.

	FREQUENCY = 1000 HZ SOURCE DEPTH = 150 M $n^2(y)$ WITH POSITIVE GRADIENT RECEIVER DEPTH						
	y = 0 meters	y = 50 meters	y = 100 meters	y = 150 meters	y = 200 meters	y = 250 meters	y = 300 meters
$\beta_o = 84°$							
$n^2(y)$	0.98010	0.98673	0.99337	1.00000	1.0066	1.0133	1.0199
$k_y^2(y)$	-0.16065	-0.041900	0.076852	0.19560	0.31435	0.43311	0.55186
$\zeta(y)$	9.0248	2.3538	-4.3173	-10.988	-17.659	-24.330	-31.001
$\beta_o = 86°$							
$n^2(y)$	0.98010	0.98673	0.99337	1.00000	1.0066	1.0133	1.0199
$k_y^2(y)$	-0.26914	-0.15039	-0.031640	0.087112	0.20586	0.32461	0.44337
$\zeta(y)$	15.119	8.4484	1.7774	-4.8936	-11.565	-18.236	-24.907
$\beta_o = 88°$							
$n^2(y)$	0.98010	0.98673	0.99337	1.00000	1.0066	1.0133	1.0199
$k_y^2(y)$	-0.33445	-0.21570	-0.096947	0.021804	0.14056	0.25931	0.37806
$\zeta(y)$	18.788	12.117	5.4461	-1.2249	-7.8959	-14.567	-21.238
$\beta_o = 90°$							
$n^2(y)$	0.98010	0.98673	0.99337	1.00000	1.0066	1.0133	1.0199
$k_y^2(y)$	-0.35625	-0.23750	-0.11875	0.0	0.11875	0.23750	0.35625
$\zeta(y)$	20.013	13.342	6.6710	0.0	-6.6710	-13.342	-20.013
$\beta_o = 92°$							
$n^2(y)$	0.98010	0.98673	0.99337	1.00000	1.0066	1.0133	1.0199
$k_y^2(y)$	-0.33445	-0.21570	-0.096947	0.021804	0.14056	0.25931	0.37806
$\zeta(y)$	18.788	12.117	0.5.4461	-1.2249	-7.8959	-14.567	-21.238
$\beta_o = 94°$							
$n^2(y)$	0.98010	0.98673	0.99337	1.00000	1.0066	1.0133	1.0199
$k_y^2(y)$	-0.26914	-0.15039	-0.031640	0.087112	0.20586	0.32461	0.44337
$\zeta(y)$	15.119	8.4484	1.7774	-4.8936	-11.565	-18.236	-24.907
$\beta_o = 96$							
$n^2(y)$	0.98010	0.98673	0.99337	1.00000	1.0066	1.0133	1.0199
$k_y^2(y)$	-0.16065	-0.041900	0.076852	0.19560	0.31435	0.43311	0.55186
$\zeta(y)$	9.0248	2.3538	-4.3173	-10.988	-17.659	-24.330	-31.001
$\beta_o = 98°$							
$n^2(y)$	0.98010	0.98673	0.99337	1.00000	1.0066	1.0133	1.0199
$k_y^2(y)$	-0.0095034	0.10925	0.22800	0.34675	0.46550	0.58425	0.70300
$\zeta(y)$	0.53386	-6.1372	-12.808	-19.479	-26.150	-32.821	-39.492

Table 20. Values of $n^2(y)$, $k_y^2(y)$, $\zeta(y)$ for different launch angles β_0 and receiver depths y.

	FREQUENCY = 50 HZ SOURCE DEPTH = 150 M $n^2(y)$ WITH NEGATIVE GRADIENT						
	RECEIVER DEPTH						
	y = 0 meters	y = 50 meters	y = 100 meters	y = 150 meters	y = 200 meters	y = 250 meters	y = 300 meters
$\beta_o = 84°$ $n^2(y)$ $k_y^2(y)$ $\zeta(y)$	1.0201 0.0013341 -4.1510	1.0134 0.0010460 -3.2546	1.0067 0.00075794 -2.3582	1.00000 0.00046983 -1.4618	0.99330 0.00018173 -0.56542	0.98660 -0.0001064 0.33097	0.97990 -0.0003945 1.2274
$\beta_o = 86°$ $n^2(y)$ $k_y^2(y)$ $\zeta(y)$	1.0201 0.0010736 -3.3402	1.0134 0.00078545 -2.4438	1.0067 0.00049734 -1.5474	1.00000 0.00020924 -0.65101	0.99330 -0.0000789 0.24537	0.98660 -0.0003669 1.1418	0.97990 -0.0006551 2.0382
$\beta_o = 88°$ $n^2(y)$ $k_y^2(y)$ $\zeta(y)$	1.0201 0.00091669 -2.8521	1.0134 0.00062858 -1.9557	1.0067 0.00034048 -1.0593	1.00000 0.00005237 -0.16295	0.99330 -0.0002357 0073344	0.98660 -0.0005238 1.6298	0.97990 -0.0008119 2.5262
$\beta_o = 90°$ $n^2(y)$ $k_y^2(y)$ $\zeta(y)$	1.0201 0.00086431 -2.6892	1.0134 0.00057621 -1.7928	1.0067 0.00028810 -0.89639	1.00000 0.0 0.0	0.99330 -0.0002881 0.89639	0.98660 -0.0005762 1.7928	0.97990 -0.0008643 2.6892
$\beta_o = 92°$ $n^2(y)$ $k_y^2(y)$ $\zeta(y)$	1.0201 0.00091669 -2.8521	1.0134 0.00062858 -1.9557	1.0067 0.00034048 -1.0593	1.00000 0.00005237 -0.16295	0.99330 -0.0002357 0.73344	0.98660 -0.0005238 1.6298	0.97990 -0.0008119 2.5262
$\beta_o = 94°$ $n^2(y)$ $k_y^2(y)$ $\zeta(y)$	1.0201 0.0010736 -3.3402	1.0134 0.00078545 -2.4438	1.0067 0.00049734 -1.5474	1.00000 0.00020924 -0.65101	0.99330 -0.0000789 0.24537	0.98660 -0.0003670 1.1418	0.97990 -0.0006551 2.0382
$\beta_o = 96°$ $n^2(y)$ $k_y^2(y)$ $\zeta(y)$	1.0201 0.0013341 -4.1510	1.0134 0.0010460 -3.2546	1.0067 0.00075794 -2.3582	1.00000 0.00046983 -1.4618	0.99330 0.00018173 -0.66542	0.98660 -0.0001064 0.33097	0.97990 -0.0003945 1.2274
$\beta_o = 98°$ $n^2(y)$ $k_y^2(y)$ $\zeta(y)$	1.0201 0.0016972 -5.2806	1.0134 0.0014091 -4.3842	1.0067 0.0011210 -3.4878	1.00000 0.00083289 -2.5914	0.99330 0.00054478 -1.6950	0.98660 0.00025668 -0.79861	0.97990 -0.0000314 0.097780

Table 21. Values of $n^2(y)$, $k_y^2(y)$, $\zeta(y)$ for different launch angles β_0 and receiver depths y.

	FREQUENCY = 250 HZ SOURCE DEPTH = 150 M $n^2(y)$ WITH NEGATIVE GRADIENT						
	RECEIVER DEPTH						
	y = 0 meters	y = 50 meters	y = 100 meters	y = 150 meters	y = 200 meters	y = 250 meters	y = 300 meters
$\beta_o = 84°$							
$n^2(y)$	1.0201	1.0134	1.0067	1.00000	0.99330	0.98660	0.97990
$k_y^2(y)$	0.033654	0.026151	0.018948	0.011746	0.0045432	-0.0026594	-0.0098620
$\zeta(y)$	-12.138	-9.5165	-6.8954	-4.2744	-1.6533	0.96776	3.5888
$\beta_o = 86°$							
$n^2(y)$	1.0201	1.0134	1.0067	1.00000	0.99330	0.98660	0.97990
$k_y^2(y)$	0.026839	0.019636	0.012434	0.0052310	-0.0019716	-0.0091742	-0.016377
$\zeta(y)$	-9.7667	-7.1457	-4.5246	-1.9036	0.71748	3.3385	5.9596
$\beta_o = 88°$							
$n^2(y)$	1.0201	1.0134	1.0067	1.00000	0.99330	0.98660	0.97990
$k_y^2(y)$	0.022917	0.015715	0.0085119	0.0013093	-0.0058933	-0.013096	-0.020298
$\zeta(y)$	-8.3396	-5.7186	-3.0975	-0.47647	2.1446	4.7656	7.3867
$\beta_o = 90°$							
$n^2(y)$	1.0201	1.0134	1.0067	1.00000	0.99330	0.98660	0.97990
$k_y^2(y)$	0.021608	0.014405	0.0072026	0.0	-0.0072026	-0.014405	-0.021608
$\zeta(y)$	-7.8632	-5.2421	-2.6211	0.0	2.6211	5.2421	7.8632
$\beta_o = 92°$							
$n^2(y)$	1.0201	1.0134	1.0067	1.00000	0.99330	0.98660	0.97990
$k_y^2(y)$	0.022917	0.015715	0.0085119	0.0013093	-0.0058933	-0.013096	-0.020298
$\zeta(y)$	-8.3396	-5.7186	-3.0975	-0.47647	2.1446	4.7656	7.3867
$\beta_o = 94°$							
$n^2(y)$	1.0201	1.0134	1.0067	1.00000	0.99330	0.98660	0.97990
$k_y^2(y)$	0.026839	0.019636	0.012434	0.0052310	-0.0019716	-0.0091742	-0.016377
$\zeta(y)$	-9.7667	-7.1457	-4.5246	-1.9036	0.71748	3.3385	5.9596
$\beta_o = 96°$							
$n^2(y)$	1.0201	1.0134	1.0067	1.00000	0.99330	0.98660	0.97990
$k_y^2(y)$	0.033354	0.026151	0.018948	0.011746	0.0045432	-0.0026594	-0.0098620
$\zeta(y)$	-12.138	-9.5165	-6.8954	-4.2744	-1.6533	0.96776	3.5888
$\beta_o = 98°$							
$n^2(y)$	1.0201	1.0134	1.0067	1.00000	0.99330	0.98660	0.97990
$k_y^2(y)$	0.042430	0.035227	0.028025	0.020822	0.013620	0.0064169	-0.0007857
$\zeta(y)$	-15.440	-12.819	-10.198	-7.5773	-4.9562	-2.3351	0.28591

Table 22. Values of $n^2(y)$, $k_y^2(y)$, $\zeta(y)$ for different launch angles β_0 and receiver depths y.

	FREQUENCY = 1000 HZ SOURCE DEPTH = 150 M $n^2(y)$ WITH NEGATIVE GRADIENT						
	RECEIVER DEPTH						
	y = 0 meters	y = 50 meters	y = 100 meters	y = 150 meters	y = 200 meters	y = 250 meters	y = 300 meters
$\beta_o = 84°$ $n^2(y)$ $k_y^2(y)$ $\zeta(y)$	1.0201 0.53366 -30.585	1.0134 0.41842 -23.980	1.0067 0.30317 -17.375	1.00000 0.18793 -10.771	0.99330 0.072692 -4.1661	0.98660 -0.042550 2.4386	0.97990 -0.15779 9.0432
$\beta_o = 86°$ $n^2(y)$ $k_y^2(y)$ $\zeta(y)$	1.0201 0.42942 -24.611	1.0134 0.31418 -18.006	1.0067 0.19894 -11.401	1.00000 0.083696 -4.7967	0.99330 -0.031546 1.8079	0.98660 -0.14679 8.4126	0.97990 -0.26203 15.017
$\beta_o = 88°$ $n^2(y)$ $k_y^2(y)$ $\zeta(y)$	1.0201 0.36667 -21.015	1.0134 0.25143 -14.410	1.0067 0.13619 -7.8053	1.00000 0.020949 -1.2006	0.99330 -0.094292 5.4040	0.98660 -0.20953 12.009	0.97990 -0.32478 18.613
$\beta_o = 90°$ $n^2(y)$ $k_y^2(y)$ $\zeta(y)$	1.0201 0.34572 -19.814	1.0134 0.23048 -13.209	1.0067 0.11524 -6.6046	1.00000 0.0 0.0	0.99330 -0.11524 6.6046	0.98660 -0.23048 13.209	0.97990 -0.34572 19.814
$\beta_o = 92°$ $n^2(y)$ $k_y^2(y)$ $\zeta(y)$	1.0201 0.36667 -21.015	1.0134 0.25143 -14.410	1.0067 0.13619 -7.8053	1.00000 0.020949 -1.2006	0.99330 -0.094292 5.4040	0.98660 -0.20953 12.009	0.97990 -0.32478 18.613
$\beta_o = 94°$ $n^2(y)$ $k_y^2(y)$ $\zeta(y)$	1.0201 0.42942 -24.611	1.0134 0.31418 -18.006	1.0067 0.19894 -11.401	1.00000 0.083696 -4.7967	0.99330 -0.031546 1.8079	0.98660 -0.14679 8.4126	0.97990 -0.26203 15.017
$\beta_o = 96°$ $n^2(y)$ $k_y^2(y)$ $\zeta(y)$	1.0201 0.53366 -30.585	1.0134 0.41842 -23.980	1.0067 0.30317 -17.375	1.00000 0.18793 -10.771	0.99330 0.072692 -4.1661	0.98660 -0.042550 2.4386	0.97990 -0.15779 9.0432
$\beta_o = 98°$ $n^2(y)$ $k_y^2(y)$ $\zeta(y)$	1.0201 0.67888 -38.907	1.0134 0.56364 -32.303	1.0067 0.44840 -25.698	1.00000 0.33315 -19.094	0.99330 0.21791 -12.489	0.98660 0.10267 -5.8842	0.97990 -0.012571 0.72045

Table 23. Values of $n^2(y)$, $k_y^2(y)$, $\zeta(y)$ for different launch angles β_0 and receiver depths y.

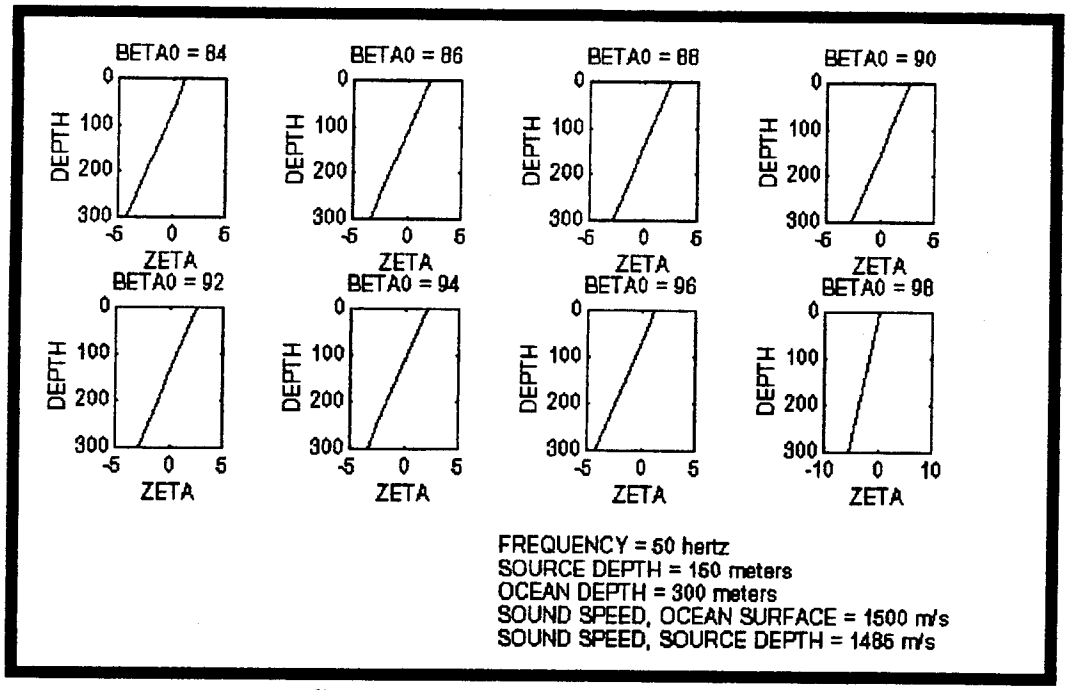

Figure 12. Plot of $\zeta(y)$ versus depth y for different launch angles β_0: $n^2(y)$ with positive gradient.

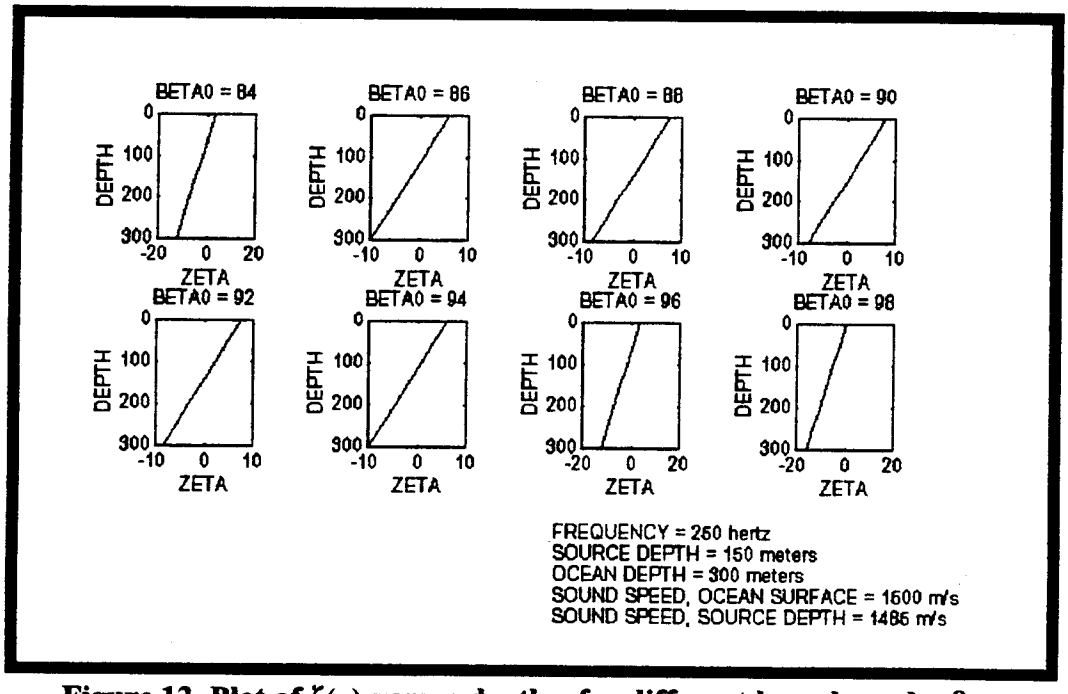

Figure 13. Plot of $\zeta(y)$ versus depth y for different launch angles β_0: $n^2(y)$ with positive gradient.

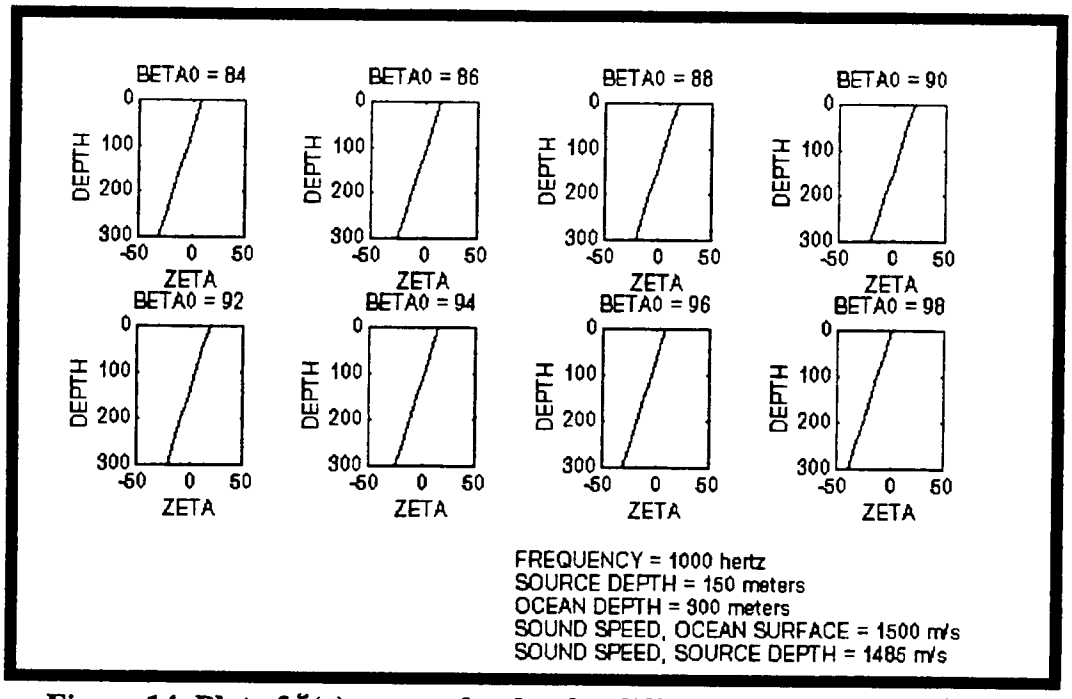

Figure 14. Plot of $\zeta(y)$ versus depth y for different launch angles β_0: $n^2(y)$ with positive gradient.

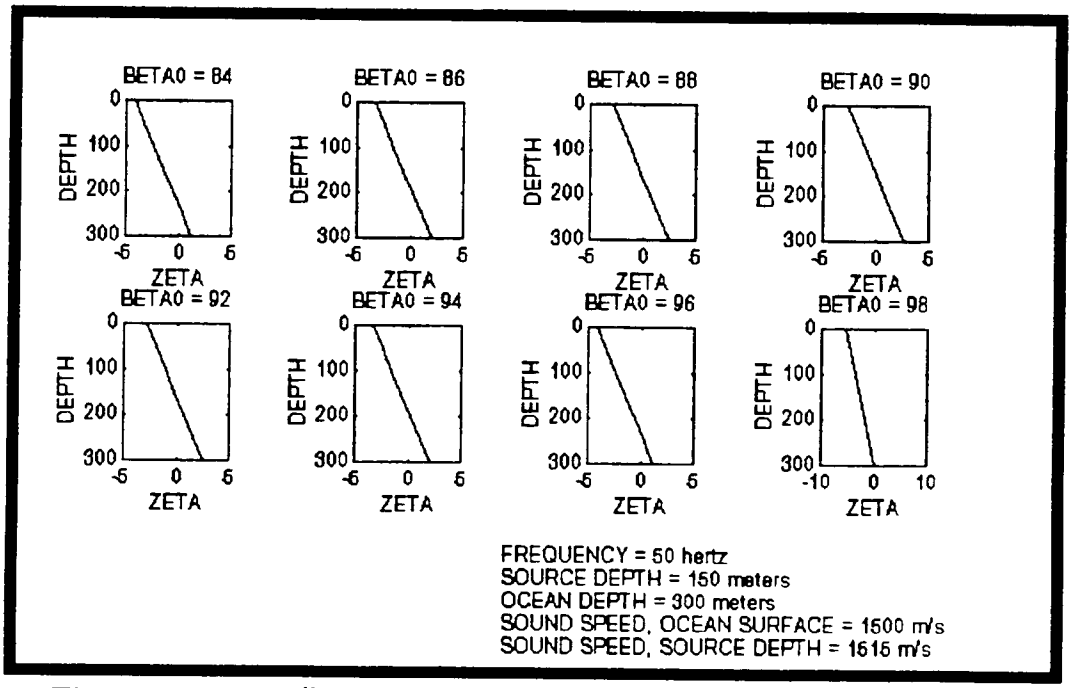

Figure 15. Plot of $\zeta(y)$ versus depth y for different launch angles β_0: $n^2(y)$ with negative gradient.

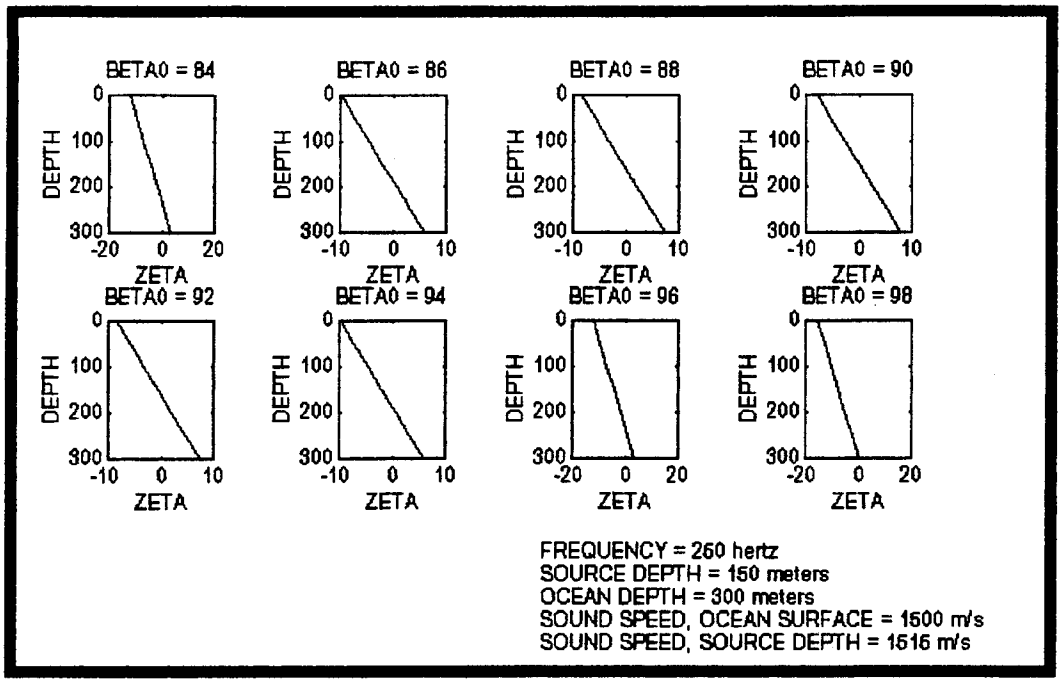

Figure 16. Plot of $\zeta(y)$ versus depth y for different launch angles β_0: $n^2(y)$ with negative gradient.

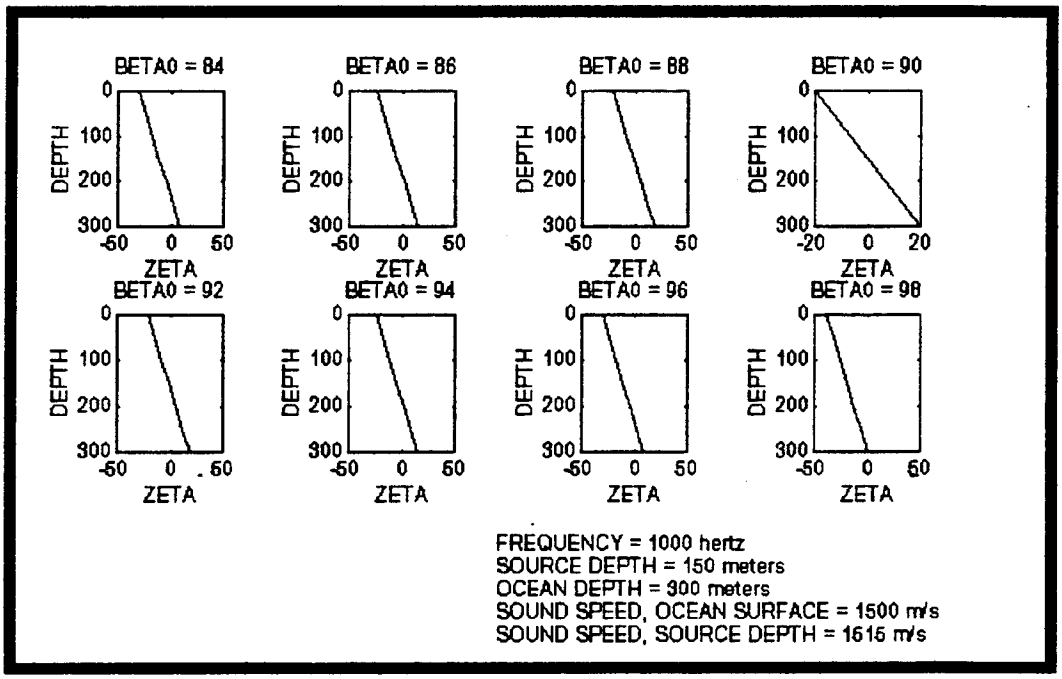

Figure 17. Plot of $\zeta(y)$ versus depth y for different launch angles β_0: $n^2(y)$ with negative gradient.

LIST OF REFERENCES

1. Boyles, A. C., *Acoustic Waveguides, Applications to Oceanic Science*, pp.: 107 - 174, John Wiley & Sons, Inc., New York, NY, 1984.

2. Ziomek, L. J., "Sound-Pressure Level Calculations Using the RRA Algorithm for Depth-Dependent Speeds of Sound Valid at Turning Points and Focal Points," submitted for publication.

3. Ziomek, L. J., "The RRA Algorithm: Recursive Ray Acoustics for Three-Dimensional Speeds of Sound, " IEEE Journal of Oceanic Engineering, v. 18, No. 1, January 1993.

4. Nayfeh, A. H., *Perturbation Methods*, p. 337, John Wiley & Sons, Inc., New York, NY, 1973.

5. Abramowitz, Milton and Stegun, Irene, *Handbook of Mathematical Functions with Formulas, Graphs, and Mathematical Tables*, Dover Publications, Inc., New York, NY, Nineth Printing, November 1970.

INITIAL DISTRIBUTION LIST

1. Defense Technical Information Center Cameron Station Alexandria, Virginia 22304-6145	2
2. Library, Code 52 Naval Postgraduate School Monterey, California 93943-5101	2
3. Chairman, Code EC Electrical and Computer Engineering Department Naval Postgraduate School Monterey, California 93943-5121	1
4. Lawrence J. Ziomek, Code EC/Zm Electrical and Computer Engineering Department Naval Postgraduate School Monterey, California 93943-5121	3
5. Clyde Scandrett, Code MA/Sd Mathematics Department Naval Postgraduate School Monterey, California 93943-5216	2
6. Robert House 139 Gwen Avenue Gallatin, Tennessee 37066	1
7. Rodney Luck 390 D Ricketts Road Monterey, California 93940	1